Purdue University
Purdue e-Pubs

Open Access Theses | Theses and Dissertations

12-2016

Mechanism of shot peening enhancement for the fatigue performance of AA7050-T7451

Daniel James Chadwick
Purdue University

Follow this and additional works at: https://docs.lib.purdue.edu/open_access_theses

 Part of the Aerospace Engineering Commons, and the Materials Science and Engineering Commons

Recommended Citation
Chadwick, Daniel James, "Mechanism of shot peening enhancement for the fatigue performance of AA7050-T7451" (2016). *Open Access Theses*. 839.
https://docs.lib.purdue.edu/open_access_theses/839

This document has been made available through Purdue e-Pubs, a service of the Purdue University Libraries. Please contact epubs@purdue.edu for additional information.

Graduate School Form
30 Updated 12/26/2015

PURDUE UNIVERSITY
GRADUATE SCHOOL
Thesis/Dissertation Acceptance

This is to certify that the thesis/dissertation prepared

By Daniel James Chadwick

Entitled

MECHANISM OF SHOT PEENING ENHANCEMENT FOR THE FATIGUE PERFORMANCE OF AA7050

For the degree of Master of Science in Aeronautics and Astronautics

Is approved by the final examining committee:

Professor Michael Sangid
Chair

Professor David Bahr

Professor Alberto Mello

To the best of my knowledge and as understood by the student in the Thesis/Dissertation Agreement, Publication Delay, and Certification Disclaimer (Graduate School Form 32), this thesis/dissertation adheres to the provisions of Purdue University's "Policy of Integrity in Research" and the use of copyright material.

Approved by Major Professor(s): Prof. Michael Sangid

Approved by: Prof. Weinong Chen 12/7/2016

Head of the Departmental Graduate Program Date

MECHANISM OF SHOT PEENING ENHANCEMENT FOR THE FATIGUE PERFORMANCE OF AA7050-T7451

A Thesis

Submitted to the Faculty

of

Purdue University

by

Daniel James Chadwick

In Partial Fulfillment of the

Requirements for the Degree

of

Master of Science in Aeronautics and Astronautics

December 2016

Purdue University

West Lafayette, Indiana

ACKNOWLEDGEMENTS

Throughout the duration of this research, I have had great assistance from numerous individuals, in a number of capacities. Firstly, I would like to express my gratitude to my Major Professor, Dr. Michael Sangid, for the opportunity to work within the ACME^2 laboratory research group, and for his constant and unwavering guidance and mentorship throughout my time at Purdue University. The opportunity to be part of ACME^2 under Dr. Sangid's leadership has been crucial in the pursuit of my advanced degree. Thank you to my lab mates for your comradery, comic relief, and expertise. Specific mentions must go to Dr. Alberto Mello, John Rotella and Andrea Nicolas, for your direct assistance in this work. I would like to thank Lena Huynh, for assistance in settling into West Lafayette. Secondly, I would like to thank my collaborative co-operators at Purdue University, of the Materials Engineering Department's Center for Surface Engineering and Enhancement (CSEE). Specifically, Dr. David Bahr, Head of Materials Engineering, Purdue University, of whom made this project possible, and PhD candidate, Siavash Ghanbari. Thanks to Mr. Jack Champagne, President Electronics Incorporated, and Mr. Jim Whalen, Progressive Surface, of whom provided significant interest and shot peening assistance towards this research project. Thanks to Dr. Mauro Sardela, Head of the Materials Research Laboratory, at the University of Illinois – Urbana Champagne. Elements of this research was carried out at the Frederick Seitz Materials Research Laboratory Central Research Facilities, University of Illinois. Finally, I would like to thank my friends and family of whom have provided sturdy support throughout my return to academic endeavors. Special mention to my close group of friends at Purdue University, Alexander Finch, Priya Ravi, Hoonigan Jin Kim, Denon Wong, Alice Liberman and Arly Black. Finally, my gratitude to the Royal Australian Air Force, for all the opportunities I have been provided throughout my career as an Aeronautical Engineering Officer.

TABLE OF CONTENTS

LIST OF FIGURES

Figure Page

NOMENCLATURE

In order of appearance.

SEM – Scanning Electron Microscope
EBSD – Electron back Scatter Diffraction
EDS – Energy Dispersive (X-Ray) Spectroscopy
XRD – X-ray Diffraction
Min Wt. % - Minimum Weight by Percentage
Max Wt. % - Maximum Weight by Percentage
2D – Two Dimensional
A, B, n, C, m, Epsilon Dot Zero – Constants from Johnson-Cook Material Model
T – Almen Intensity Exposure Point (Passes)
2T – Almen Intensity Exposure Point (Passes)
CNC – Computer Numerical Controlled
λ – Wavelength
d – Lattice Spacing
CI – Confidence Index
S – X-Ray Source
D – X-Ray Detector
2θ – Diffraction Angle
N – Angle between incident and diffracted beam bisector, and the normal of the surface
Ψ – Orientation of sample angle
v – Poisson's Ratio
E – Elastic (Young's) Modulus
$\sigma\phi$ – Stress (residual)
R – Stress Ratio
ε – Strain

n – Number of Fatigue Cycles (also positive integer in Bragg's Law equation)

P – Indent Force

C – Measure of curvature on loading ramp of load/depth curve (compliance)

h – Indent Depth

ABSTRACT

Chadwick, Daniel J. M.S.A.A., Purdue University, December 2016. Mechanism of Shot Peening Enhancement for the Fatigue Performance of AA7050-T7451. Major Professor: Dr. Michael D. Sangid.

Shot peening is a dynamic cold working process involving the impingement of peening media onto a substrate surface. Shot peening is commonly employed as a surface treatment technique within the aerospace industry during manufacturing, in order to improve fatigue performance of structural components. The compressive residual stress induced during shot peening is understood to result in fatigue crack growth retardation, improving the performance of shot peened components. However, shot peening is a compromise between the benefit of inducing a compressive residual stress and causing detrimental surface damage. Due to the relatively soft nature of AA7050-T7451, shot peening can result in cracking of the constituent particles, the effect of which is recognized as a 'critically detrimental influence upon the component's fatigue performance.'[1] The intention of this thesis is to understand the balance and fundamentals of these competing phenomena, through analysis involving a comparative study throughout the fatigue life cycle of 'as manufactured' versus shot peened AA7050-T7451. A series of dog bone samples were manufactured, with a subset undergoing shot peening surface treatment. Microstructural grain characterization and comparison of 'as manufactured' and shot peened AA7050-T7451 has been carried out using scanning electron microscope (SEM), electron back

scatter diffraction (EBSD), and energy dispersive spectroscopy (EDS) techniques. A residual stress analysis through interrupted fatigue of ‘as manufactured’ and shot peened AA7050-T7451 was completed utilizing a combination of x-ray diffraction (XRD) and nano-indentation. The fatigue life cycle performance of the ‘as manufactured’ versus shot peened material has been evaluated, including qualitative analysis and comparison of crack initiation and propagation in ‘as manufactured’ and shot peened material. Through this experimentation and analysis, this thesis endeavors to answer the question of what is the mechanism for shot peening enhancement for fatigue performance. An objective of this work is to understand how a cracked particle starts to incubate the short crack into the matrix within a residual stress field.

CHAPTER 1. INTRODUCTION

The link between material processing and material performance has been exploited by mankind since his inception. Throughout history, mankind has sought to improve the performance of metallic tools, weapons and components. Whilst the microstructural effects may not have been fully understood by early metallurgist and blacksmiths, the intrinsic link between material processing and material performance has been ever present. This study concentrates upon the modern day surface treatment technique, shot peening. A technique that has evolved from the principles of primitive forms of cold working, and now finds itself relevant in today's highly regulated aerospace industry.

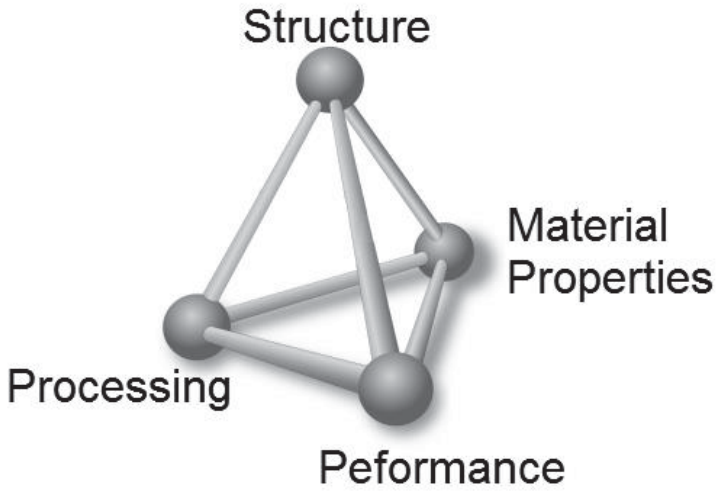

Figure 1 Fundamentals of material behavior; the structure, processing, material properties, and resultant performance.

Shot peening is a surface treatment conditioning technique developed in the late 1920s, of which has drawn upon the cold working processes throughout history. Shot peening is a dynamic collision process between shot (consisting of metallic, glass, or ceramic spheres) and substrate (the treated component), resulting in plastic deformation of the substrate and a compressive residual stress region adjacent to the area of impact. Essentially, controlled cold working by thousands of small impingements of shot media.

According to Bush *et al*[2], the earliest ancient examples of cold working include hammering. A gold helmet seen at Figure 1, retrieved from the Mesopotamian ancient city of Ur showing evidence of the process, is dated *circa* 2700 B.C.

Figure 2. An early example of cold working, a gold helmet manufactured *circa* 2700 B.C.[3]

Throughout the ages, the consistent principle of cold working processes is the subjection of material to mechanical stress in order to induce plastic deformation, and thus, a permanent change to the microstructure of the crystalline lattice, and consequently, the material's performance. William Shenk, a turn of the twentieth century blacksmith, was amongst the first to utilize the peening hammer.[4]

The evolution of shot peening, into the practice we recognize today, occurred in earnest through the twentieth century. Shot peening was introduced in the United States around the 1930s, with patents being granted for the shot peening machine in 1934.[5] The practice was largely utilized during manufacturing throughout the Second World War era, with applications including the enhancement of the fatigue life on components such as leaf springs, connecting rods, crankshafts, camshafts, and aircraft landing gear structure. It was not until the close of the Second World War, 1945, when the precise measurement of shot peening was mastered by John Almen, with the 'Almen strip' method used to measure

peening intensity. Whilst early in the development of cold working, the benefits of the process were recognized, it was not until this significant development in the art of shot peening at the middle of the twentieth century that the fundamental science behind the process was grasped.

The intention of this study is to better understand the microstructural effects of shot peening through a number of different experimental techniques. With experimentation and analysis centered on a comparison between ‘as manufactured’ aerospace grade aluminum alloy, AA7050-T7451, and ‘shot peened’ samples of identical material, the difference in material behavior as a result of the shot peening process is key. In this research, microstructural grain characterization and comparison of ‘as manufactured’ and shot peened AA7050-T7451 will be carried out using scanning electron microscope (SEM) in combination with electron back scatter diffraction (EBSD) equipment. This technique will enable the acquisition of data on grain orientation, sizing, and shape, for statistical comparison. In order to carry out elemental analysis of constituent elements of the material, including secondary phase identification, energy dispersive spectroscopy (EDS) will be employed. The intention of this practice is to positively identify precipitate particles, in order to carry out specific analysis and experimentation through nano-indentation hardness testing, and SEM imaging. It is hypothesized that the hardness of precipitates, their potential cracked state from peening, may contribute significantly toward the fatigue performance. A qualitative survey of precipitate particles before and after shot peeing is carried out, in addition to before and after fatigue cycling each case. Additionally, x-ray diffraction is employed to evaluate the residual stress (average near surface compressive residual stress magnitude) throughout fatigue cycling of samples.

Through this experimentation, this thesis endeavors to answer the question of what is the mechanism for shot peening enhancement for fatigue performance. An objective of this work is to understand how a cracked particle starts to incubate the short crack into the matrix within a residual stress field, and at what stage of the fatigue life this occurs, and if shot peening has an effect upon the phenomenon.

CHAPTER 2. LITERATURE REVIEW

2.1 Background

Shot peening is a dynamic work hardening surface treatment process. The process involves inducing a compressive residual stress into a material, thus modifying the material's microstructure and subsequent performance. The relevant literature will be presented in order to illustrate the current state of the process. Additionally, throughout this research, the experimental methodology and conventions associated with the processes draw upon the advances of existing literature. A previous study, conducted by Sharp and Clarke, will be reviewed and summarized in relevance to this research, in addition, the findings of a preliminary finite element model developed by the researcher, will be presented.

2.2 Fundamentals of Shot Peening

Kirk[6] breaks down the fundamentals of shot peeing into the following topic areas; shot peening basics, peening media, residual stress distribution, coverage and saturation. An elegant analogy compares shot peening to spray painting. In that 'roughly spherical particles are projected onto to a surface with the object of achieving a uniform, specified coverage…with particles accelerated by compressed air from a gun.'[7] With 'a spray cone produced whose intensity (particles crossing a unit area per unit time) decreases as the square of the distance from the gun to the work piece… the greater the volume of paint emerging from the gun per unit time, the greater the application.'[8]

2.2.1 Residual Stresses

The key modification of a material, through the shot peening process, lies in the inducing of a compressive residual stress at the surface. Kirk states that 'the object of that compressive layer is to offset applied tensile stresses, thus improving service performance (fatigue, corrosion-fatigue etc.).'[9] The compressive residual stress is attributed to the plastic deformation of the substrate, suffered during the peening process. According to Elber, 'when a material is shot peened, the residual compressive stresses at the surface prolong the fatigue life.'[10] In a specific study by Kirk, the residual stress in shot peened components, it is stated that the 'shot peening of components produces a magic skin containing compressive residual macro-stress…skin has a thickness that is largely determined by the size of the shot particles which have been used.' Kirk attributes the residual stress to 'overlapping stress fields from numerous indentations.'[11] Put more simply, when peening media hits the substrate, it causes plastic deformation, stretching the impacted area. When the surface of the substrate is covered in these small deformations, there is a continuous layer of compressive stress adjacent to the peened surface.[12] It is widely accepted that it is this effect of compressive residual stress is the mechanism by which shot peening extends fatigue life. This is backed up by significant experimental evidence within literature.

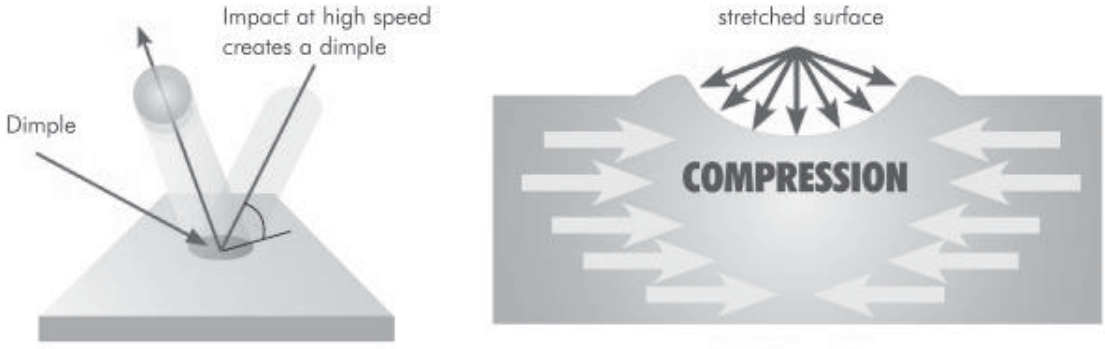

Figure 3 Shot peening causing plastic deformation and inducing a compressive residual stress region adjacent to the impacted surface.[13]

2.2.2 Depth of Compressed Layer and Stress Relaxation

In order to appropriate a shot peening process, it is critical to quantify the depth, and magnitude of the compressive residual stress region induced by peening. The depth and magnitude of the compressive residual stress can be quantified using numerous destructive and non-destructive methods testing methods such as x-ray diffraction, slitting, drilling, or nano-indentation. Kirk states that the depth and magnitude of the compressive residual stress region varies with peening intensity, as well as the hardness of the substrate material.[14] Peening 'intensity' is quantified though a technique known as the Almen intensity test. The compressive residual stress is critical in the enhancement of fatigue life. It should be noted that the shot peening process is only beneficial in delaying cracking in high cycle fatigue. This is due to stress relaxation during the crack propagation phase observed during low cycle fatigue, where due to this relaxation, the induced surface damage caused by shot peening outweighs the marginalized crack retardation caused by compressive residual stress.

2.2.3 Shot Media

In order for the shot to impart a perfect collision with substrate, Kirk states that 'batches of shot would comprise perfectly spherical particles, all of identical diameter, having infinitely high hardness, and fracture resistance.'[15] However in reality such materials do not exist. Subsequently, materials selected for shot are endeavored to emulate this desired state, and shot is thus usually comprised of ceramics, glass, or cast iron. An added complication of the choice of shot material is fracture toughness, whereby 'if the shots kinetic energy is greater than the work required to fracture it, then it will break.'[16] Subsequently, for predominantly non-ferrous materials, such as AA7050, of which broken shot embedding/contamination of ferrous material is of concern, then the ceramic or glass alternatives are employed as preferred shot media.

2.2.4 The Effect of Peening on the Fatigue Life of AA7050

A relevant study to this research is the work of P.K. Sharp and G. Clark, of the Airframes and Engines Division, Aeronautical and Maritime Research Laboratory, of the Defence Science and Technology Organization (Australia). Sharp and Clark investigate the effect of peening on the fatigue life of 7050 aluminum alloy, with the intention of 'establishing a life-improvement-factor'[17] for components subjected to shot peening for structural use on the F/A-18 Hornet aircraft, of the Royal Australian Air Force.

Sharp and Clark discuss the implications of highly optimized structural design of high performance military aircraft, including the 'increased sensitivity of airframe structure and its fatigue life to surface features such as corrosion and mechanical damage.'[18]

It is discussed that shot peening treatments are 'widely used in mechanical and aeronautical engineering to improve the fatigue performance of components,'[19] however it is also acknowledged through citing the work of Clayton and Clark[20] that shot peening can, in some cases, result in a decrease in fatigue life.

The work of Sharp and Clark goes on to describe the two most significant parameters associated with the shot peening process, as coverage (proportion of surface area peened) and saturation (amount of peening energy applied to each area). It is stated that these two factors primarily contribute to the effect upon improving the fatigue life for a given applied loading. These primary factors are said to be calibrated, or quantified, via the aforementioned Almen Intensity test.

2.2.4.1 Almen Intensity Test

The Almen Intensity is a shot peening specific metric developed by J.O. Almen, the pioneer of the shot peening quantification practice. Almen developed the 'Almen Strip', which is a thin piece of SAE1070 steel, used to essentially culminate numerous variables/parameters involved in the shot peening process. It is stated that the 'calibration of the impact energy, or peening intensity (via the Almen Intensity) of the shot stream is essential for controlled shot peening... and the energy of the stream is a function of the media size, material, hardness, velocity, and impingement angle.'[21] Broulidakis[22] provides a concise summary of the Almen Intensity, stating that it is defined as the arc height of the Almen strip, following the peening process. The Almen arc height measurement is taken from the deflection of the strip from the base following the peening process, directly translating into Almen intensity, measured in inches.

Figure 4 The Almen strip of the Almen Intensity test, fixed in position prior to being exposed to shot peening.[23]

Sharp and Clark explain the theory behind the shot peening process inducing a compressive residual stress. Stating ‘peening attempts to spread material near the impact point against the resistance of neighboring material, thus introducing a complex subsurface stress distribution...in which the surface is in elastic compression...there is a transition to elastic tension at a deeper level.’ Figure 5 illustrates the resultant residual stress state of a substrate material, following the shot peening process.

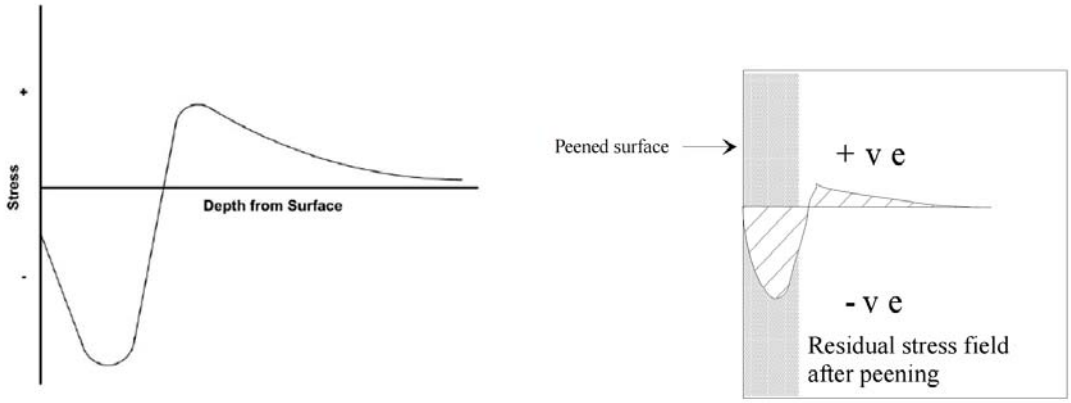

Figure 5 Schematic of residual stress distribution below a peened surface. Residual stress profiles demonstrate the compressive region adjacent to the surface caused by peening, transitioning into a deeper tensile region to maintain a state of equilibrium.[24]

Sharp and Clark draw attention to a key element of this study in their research, specifically, the tradeoff between surface damage sustained by shot peening, and the residual stress produced to benefit fatigue life. It is stated that for 'steel components the fatigue life is influenced principally by the distribution of residual stress...similarly in aluminum alloys...the residual compressive stresses are also a major component in determining fatigue life; but because of the greater damage to the softer material, the surface finish (roughness and defects) is also recognized as a critical influence on fatigue life.'[25] It is this effect, currently not well researched, on which this study will concentrate.

2.3 Material Information

The material utilized throughout this study is an aerospace grade aluminum alloy, AA7050. The material is tempered in the T7451 condition and produced in plate form, according to specification AMS 4050: AA7050-T7451,[26] and as per MIL-HDBK-5.[27] AA7050 is widely utilized within aerospace applications due to its combination of strength, toughness, and stress corrosion cracking resistance. According to Alcoa[28] of whom is a major manufacturer of the material, typical aerospace applications for AA7050-T7451 include fuselage frames, bulkheads, and wing skins.

As per MIL-HDBK-5, AA7050 is an 'Al-Zn-Mg-Cu-Zr alloy developed to have a combination of high strength, high resistance to stress corrosion cracking.' The material constituents provide a 'low sensitivity to quench, which results in high strength in thick sections.' The chemical composition limits of AA7050 by weight percent is broken down at Table 1.

Table 1 Aluminum Alloy AA7050-T7451 Chemical Composition

Chemical Composition Limits of AA7050-T7451[29]		
Element	Min Wt. %	Max Wt. %
Aluminum	87.3	90.3
Chromium		0.04
Copper	2	2.6
Iron		0.15
Magnesium	1.9	2.6
Manganese		0.1
Silicon		0.12
Titanium		0.06
Zinc	5.7	6.7
Zirconium	0.08	0.15
Other (each)		0.05
Other (total)		0.15

Further to the chemical composition of the material, the basic mechanical and material properties of AA7050-T7451 is sourced from literature, and can be seen at Table 2.

Table 2 Mechanical and Material Properties of AA7050-T7451

Properties of AA7050-T7451[30]	
Ultimate Tensile Strength	524 MPa
Yield Tensile Strength	469 MPa
Elastic Modulus	71.7 GPa
Poisson's Ratio	0.33
Density	2.83g/cc
Fracture Toughness (S-L Direction)	28 MPa-m^1/2
Fracture Toughness (T-L Direction)	31 Mpa-m^1/2
Fracture Toughness (L-T) Direction	35MPa-m^1/2

2.4 Finite Element Model

A previous study, conducted by Chadwick[31] focused upon the prediction of residual stress in an AA7050-T7451 substrate following shot peening. The intention of the study was to develop a two-dimensional (2D) axisymmetric model for the qualitative prediction of through thickness residual stress profile from the shot peening process. The modeling was carried out in software package ABAQUS, taking into account numerous variables involved, specific to the shot peening process. The variation of mechanical properties and characteristics of the substrate can be modelled in order to predict changes to substrate and material behavior resulting from the shot peening process (i.e. the residual stress profile), derived from a number of variables involved in the process. The accurate prediction through finite element modelling of the shot peening process, and resultant substrate material characteristics, can be of significant influence towards the better understanding of material final performance.

The finite element model developed is a 2D axisymmetric model for the qualitative prediction of residual stress in a substrate from a single impact of shot. The residual stress profile of a substrate following the shot peening process is a function of the variables of shot peening, including: part geometry, shot and substrate material, shot velocity, amongst others.

The model produced in the analysis represented a substrate material AA7050-T7451, and rigid body steel shot. The material and physical properties for which were sourced from literature. Figure 6 illustrates the selected area of interest for analysis, with assumptions of symmetry.

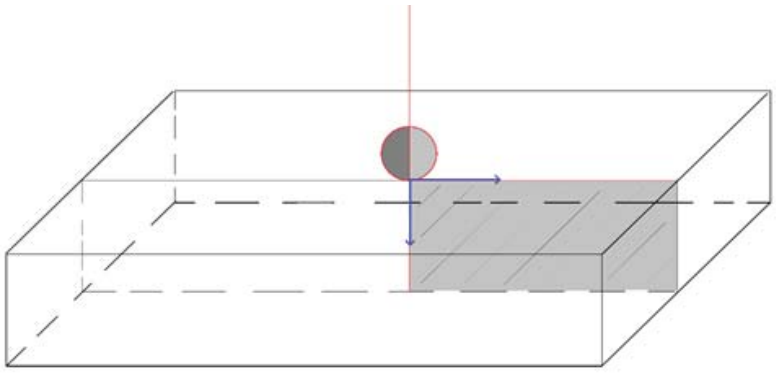

Figure 6 Substrate target and shot representative of the shot peening interaction. The light grey area illustrates the area of analysis for the 2D axisymmetric model.

The model was created using a dynamic explicit collision, with two parts created to simulate the substrate and the shot, due to the axisymmetric nature of the defined problem. The first part consisted of a 2D deformable planar shell with partitions in the upper left impact region to aid with mesh refinement. This rectangular shell was a representation of the shaded grey area of interest of the Figure 6 (where residual stress profiling following impact is prominent), and demonstrative of the cross section at the gauge of a sample geometry.

The second part represented the shot, a 2D deformable planar shell of a semi-circle representative of typical shot geometry.

2.4.1 Model Physical and Material Properties

Physical and material properties utilized to define the shot and substrate can be seen in the table below. The substrate and shot were modelled utilizing vastly different material properties. The modelling of the substrate (simulating homogeneous Aluminum Alloy AA7075-T7451) was modelled utilizing elastic-plastic material deformation model Johnson-Cook, and rate dependent hardening (Johnson-Cook). The shot (steel) was modelled as a rigid body. The properties utilized in the modelling can be seen in the below

tables. As ABAQUS is a unit-less software package, careful attention was paid to conversion and input of scientific metric units.

Table 3 Physical and Material Properties

Substrate	
Material	AA7050-T7451
Young's Modulus (GPa)	71.7
Poisson's Ratio	0.33
Density (kg/m3)	2830
Thickness (mm) (m)	1.6 (0.0016)
Shot	
Material	Steel
Diameter (mm) (m)	0.36 (0.00036)
Density (kg/m3)	7860
Mass (kg)	1.92E-7
Velocity (m/s)	55

It should be noted that typical shot peening velocities[32] range in practice from 40m/s to 70m/s so for the purpose of this model, an average velocity of this range was adopted (55m/s). This was the shot velocity utilized by Howard, and will make for simpler validation of results.

Table 4 Johnson Cook Material Modeling Constants for AA7050-T7451 including rate dependent hardening.[33]

A	B	n	C	m	Epsilon Dot Zero	Temp Trans (Deg C)	Temp Melt (Deg C)
435.7E6	2534.624E6	0.504	0.019	0.97	1	25	635

2.4.2 Model Setup

The simulation of the shot peening scenario was modelled using a dynamic explicit collision. The contact of the shot to the substrate was managed through ‘surface-to-surface’ explicit contact, with ‘normal’ behavior, and ‘hard’ contact. Surfaces of contact were defined and assigned sets (as seen in Figure 7), to control the interaction, and default automatic stabilization was set.

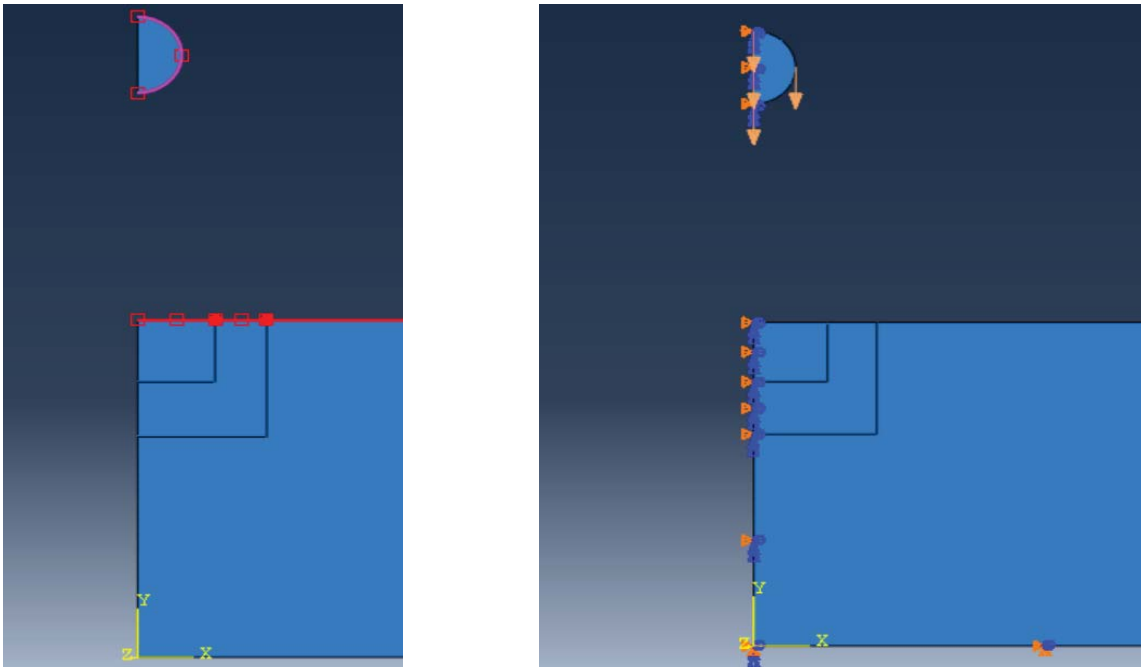

Figure 7 (Left) The defined surface ‘contacts’ of the shot and substrate, and (Right) the assembly of the 2D axisymmetric shot peening simulation illustrating boundary conditions of axis symmetry and predefined velocity vector (55m/s) of shot.

A step duration of 9e-5 seconds was created for the interaction, based on the distance for the inbound shot to translate at its prescribed velocity, as well as ensure contact between substrate and shot, and separation. The field output interval was set at 25, which iterated and output field data at even time points of the duration of the explicit model.

The ‘initial’ step involved the creation of boundary conditions which included x-axis symmetry along the left hand side of both the shot and substrate parts, and the fixing of the

base and right hand side of the substrate (sides displacement fixed in horizontal displacement and rotation, base fixed in vertical displacement and rotation. This setup appropriately simulated a 2D configuration of clamping the dog bone into position during a shot peening process, whilst also reducing the computational overhead by assuming axis symmetry. Additionally, a 55m/s ‘predefined’ velocity field was applied to the node set of the shot, as well as mass inertia. For aesthetic purposes of modelling, the shot was placed in initial position 2.5x its diameter (a distance of 0.9mm) above the substrate, to which it would translate inbound, contact, and then separate all within the step time duration.

Both the substrate and shot parts were meshed utilizing 2-D explicit CPE4R, a 4-node bilinear plane strain quadrilateral, reduced integration, with hourglass control. This element type was recommended by ABAQUS for dynamic contact simulations, with post processing involving residual stress analysis.

The partitions of the substrate allowed for refining of the mesh adjacent to the point of surface-to-surface contact, whilst reducing the computational requirements for areas of minimal interest. Additionally, attention was closely paid to matching the element size involved in the surface-to-surface contact for best results. The mesh shape was appropriate given the geometry of the parts and contact surfaces. Further study, the potential of utilizing a 2D plane strain wedge element could be entertained for meshing of the shot (due to curved geometry of interfacing collision surface).

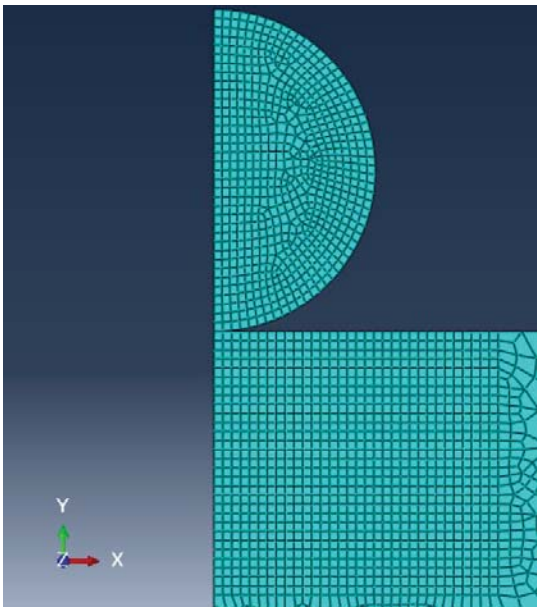

Figure 8 Mesh of shot and substrate, illustrating the refined mesh of both, in surrounds of surface to surface contact, and subsurface area of interest for residual stress profiling (substrate), seed sizing 8E-006 for refined mesh area.

Seed size was varied for the collision area locally in order to complete a convergence study. This involved varying both the local seed size of the partitions within the substrate as well as the shot. Throughout this variation, the elements on both the contact surfaces were maintained at similar sizing for compatibility. Seed size was reduced iteratively, as the principle stresses at a constant point began to converge. A total of six different mesh sizes were refined and computed, with output gained from node queries of which the locational was kept constant for comparison during convergence analysis. Using this methodology, the model stress variation could be analyzed in order to see convergence on an accurate solution (stabilizing). The convergence analysis was conducted utilizing a set of 6 refinements, incrementally decreasing in step size based on the magnitude of the delta between the results of the preceding steps. Specifically, the seed size at the convergence study deemed to be acceptable due to stabilization of stress value outputs (seed size of substrate and shot of 8.00E-6) was selected, due to convergence.

Figure 9 illustrates the variation of S11 direction stress at a stabilized step following collision at time of final iteration (25), and the convergence on a solution with variation of seed sizing.

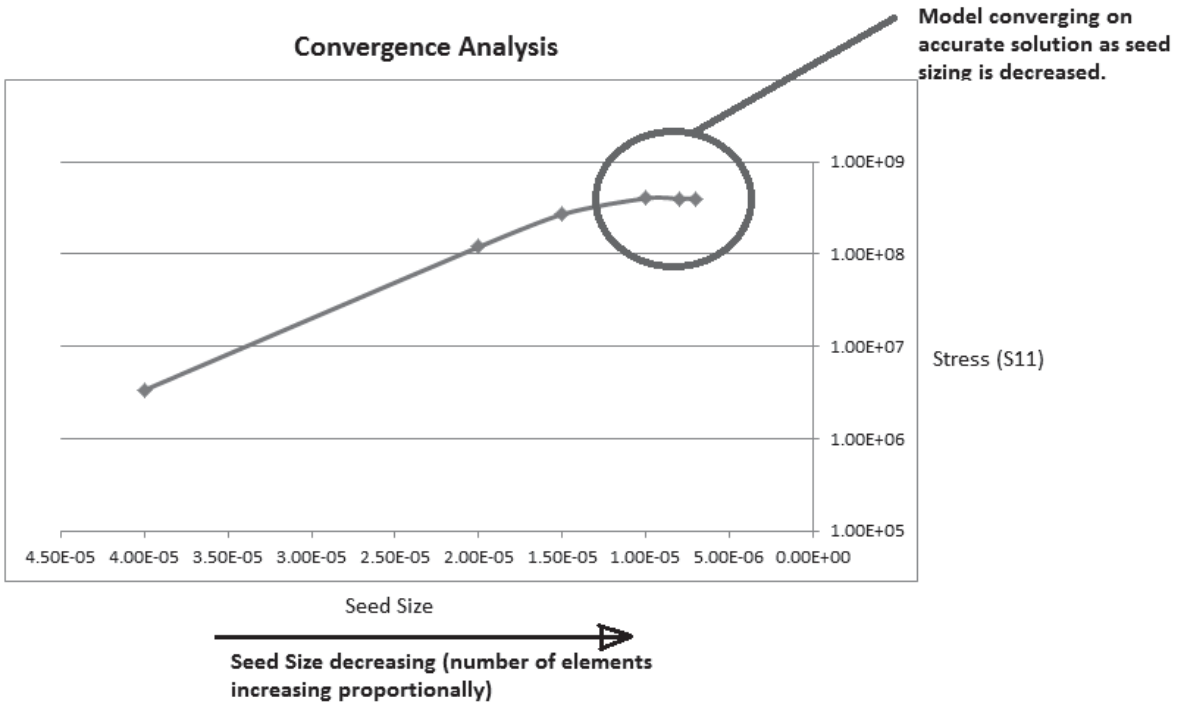

Figure 9 Convergence Analysis illustrating the relationship between solution accuracy (stabilization of output (principle stress)) and the seed size and number of elements. It can be seen that decreasing seed size, increasing the number of elements meshed, increases the accuracy of the solution.

Figure 10 illustrates the stress contour plot (through thickness direction principle stress of the substrate) following impact from the shot. As expected, there is a compressive stress adjacent to the surface-to-surface contact area of the shot and the substrate, consistent with the outcomes of literature and analytical solutions. The output stress contour demonstrates that the elastic-plastic (Johnson-Cook) rate dependent material modelling of the substrate is effective (showing strain and plastic deformation immediately adjacent to the impact on the substrate). The result was deemed qualitatively accurate.

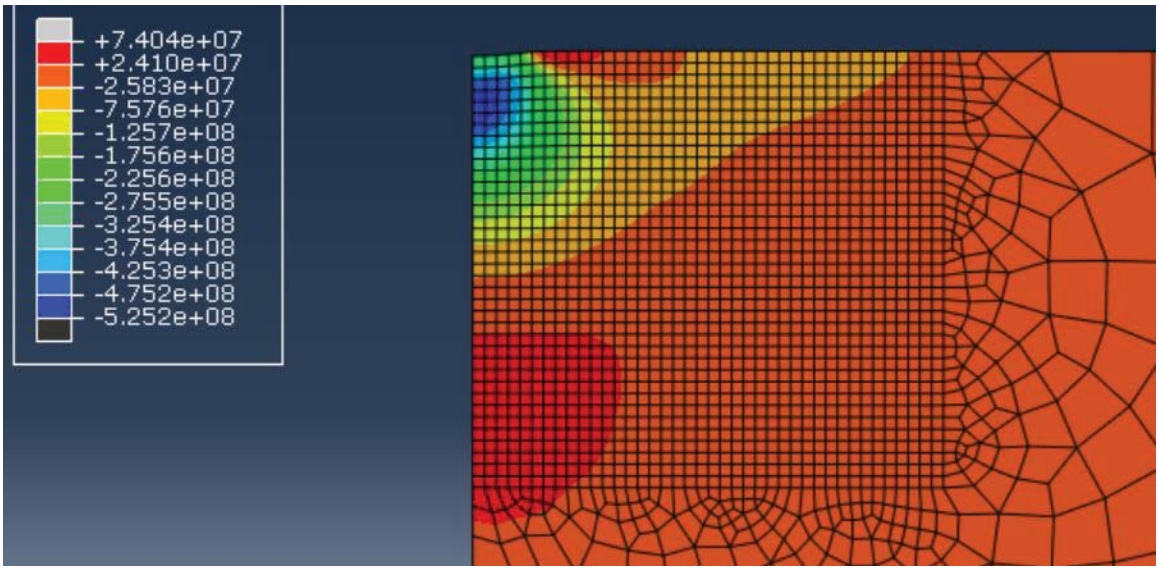

Figure 10 Through thickness stress contour plot (principle stress) of substrate following 55m/s collision with shot, demonstrating residual compressive stress resulting from the cold working process, a realistically conceivable residual stress profile, consistent with researched literature.

The qualitative variation of through thickness residual stress magnitude due to the shot peening process is well known and documented. It is expected that there is a compressive stress adjacent to the surface-to-surface contact area of the shot and the substrate, and this balanced by tensile stress through the gauge thickness.

The resulting output of the generated model is consistent with the typical qualitative residual stress profile accepted in literature, where we see a compressive stress adjacent to the surface-to-surface contact area of the shot and the substrate.

This model endeavor produced a two-dimensional (2D) axisymmetric model for the qualitative prediction of through thickness residual stress profile from the steel shot peening of AA7050-T7451. The results have been shown to have qualitative similarity with literature,[34] as well as typical qualitative theoretical residual stress profiles.

CHAPTER 3. EXPERIMENTATION

3.1 Sample Manufacture

From the plate material AA7050-T7451, a set of 20 dog bone samples were machined from a rolled plate in the L-T direction. The orientation can be seen at Figure 11, adapted from Mello, *et al.* [35]

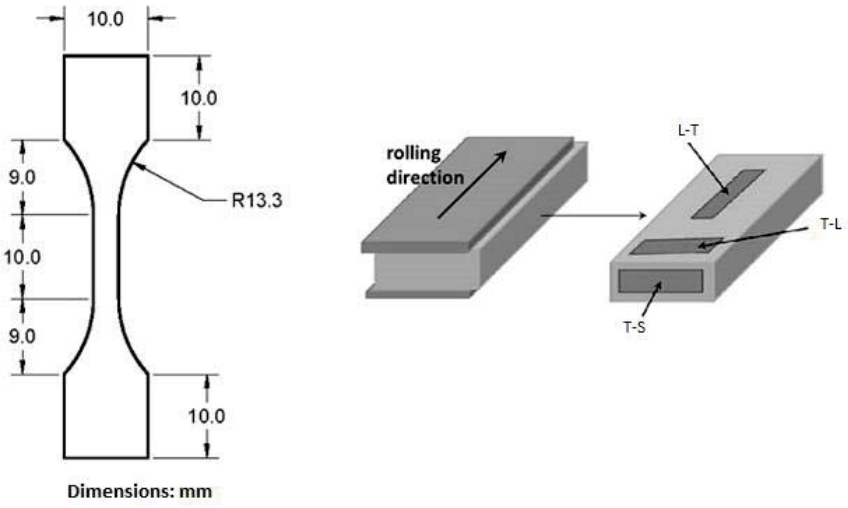

Figure 11 Orientation of the machined dog bone samples of AA7050-T7541, L-T, parallel to the rolling direction of the plate.

The AA7050-T7451 samples utilized throughout this study were the same as used by Mello, *et al*. The samples have a nominal thickness of 1.6mm and a 3mm thick gauge section. The samples have a length of 48mm. A 10x10mm section at each end gives the distinctive dog bone appearance, with this grip section utilized during fatigue loading for load cell grip - specimen load transfer. According to Mello, *et al*, the specimen were 'adapted from the ASTM E8[36] standard…and the geometry of the specimens chosen based

on the size of the surface to be analyzed and compatible dimensions with the scanning electron microscope (SEM) chamber.' Additionally, 'during machining, the specimens were machined 6.4mm away from the plate surfaces to avoid the excessive effect of the rolling processes.'[37] The effect of the rolling process affects microstructural grain orientation and texture can be observed in Figure 12, from literature.

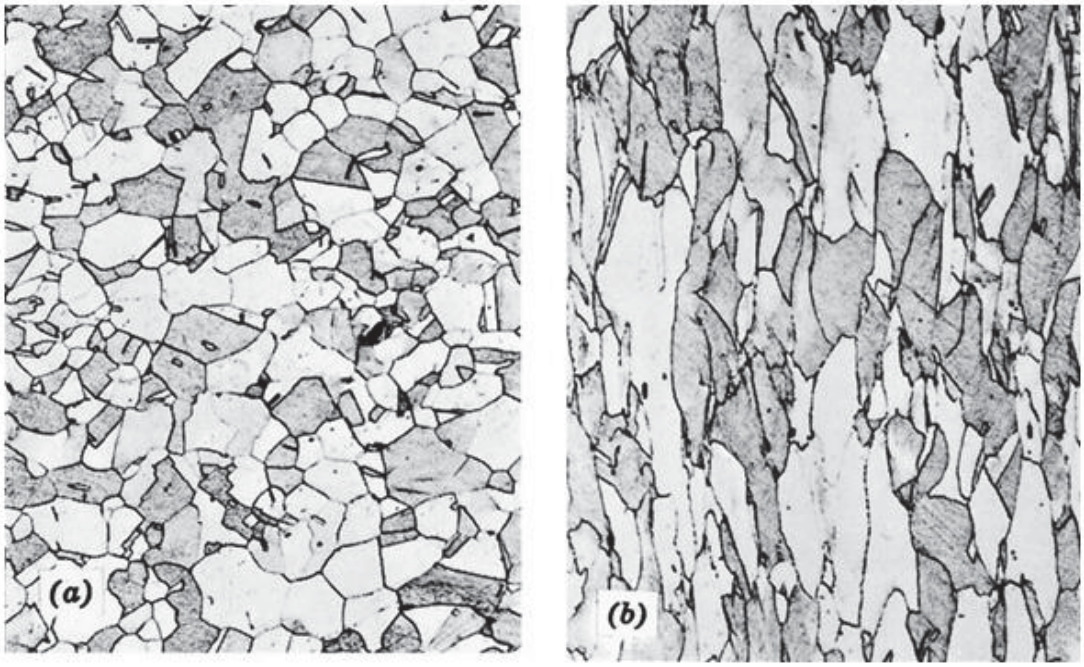

Figure 12 An example of grain texturing (a) before and (b) after rolling. Elongation of grains in (b) demonstrate rolling direction. [38]

Following the machining process, the surface of the samples exhibited significant machining evidence. The state of the surface of the AA7050-T7541 samples can be seen in Figure 13.

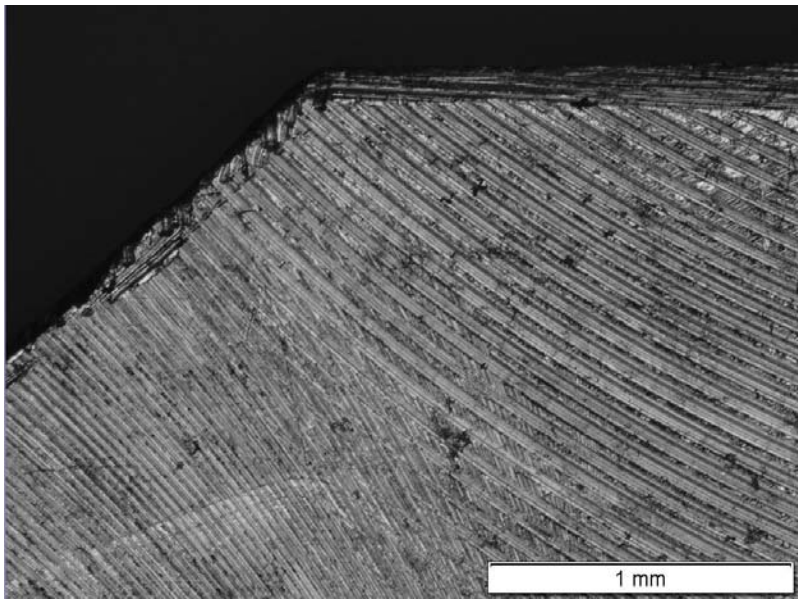

Figure 13 AA7050-T7541 radius and grip area interface exhibiting rough surface condition due to CNC machining tool manufacturing.

The decision was made to accept this ‘as manufactured’ surface condition as the baseline condition for comparison of the two sample sets, in order to replicate the most unruly of manufacturing processes. One side of all samples were roughly polished utilizing a fixed speed Buehler Ecomet V Grinder-Polisher, and a 1200 grit sand paper for 2 minutes under lubrication with water. This process gave the samples an asymmetric surface face condition, with one face in the ‘as manufactured’ condition with machining marks evident, and the opposite face, relatively free of machining marks but fine scratches as a result of the 1200 grit sand paper polish.

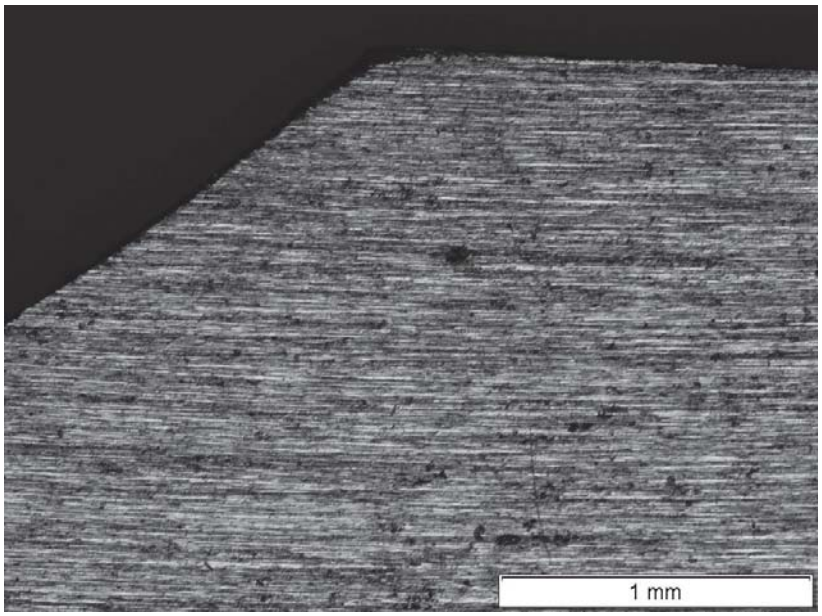

Figure 14 AA7050-T7541 radius and grip area exhibiting surface condition following 2 min 1200 grit polish.

At this point, five of the 20 samples were sent to Progressive Surface via Electronics Inc (external entities providing shot peening services) to undergo the shot peening surface treatment process. Throughout this research, these five samples shall be referred to as the 'shot peened' subset. The remaining samples were left in this condition for later experimentation and analysis, and these samples shall be referred to as the 'baseline' subset.

3.2 Shot Peening Process

3.2.1 Background

For the purposes of this experimentation, five dog bone samples of AA7050-T7451 underwent a shot peening process. The shot peening processes was outsourced to Progressive Surface via Electronics Inc. Samples were shot peened on all faces, in a staged peening process involving fixing the samples onto a flat backing whilst the opposite side was peened. The peening media utilized for shot was a Z150 ceramic zirconia, with

constituents including ~68% Zirconia (ZrO_2) and ~32% vitreous phase (SiO_2 and Al_2O_3). The shot particle size ranges from 100-210um diameter. The shot was pressure blasted through a 5/16" V-type nozzle at a pressure of 6 PSIG, with a 45 degree angle of impingement from the horizontal surface, and a 6" standoff distance. To quantify the peening parameters, saturation tests were carried out on two Almen Intensity test strips prior to the process. Exposure was measured as 'number of passes' over the test strip, and the resultant arc height, (in) was recorded. The following results were observed:

Table 5 Electronics Inc. Almen test strip results (Saturation Curve)

Exposure (# passes)	8	16	32	64
Arc Height (in)	4.3	5.5	6.1	6.6

The T and 2T parameters (the first point on the Almen saturation curve at which an increase of less than 10% in arc height is observed following a doubling of exposure), was at the 22.4 and 44.8 pass. This point is defined as peening 'saturation', whereby it is the earliest point on the curve where doubling the exposure produces no more than 10% increase in arc height. Results of the saturation curve produced by Electronics Inc. gave a T of 22.4 and 2T of 44.8 passes respectively.

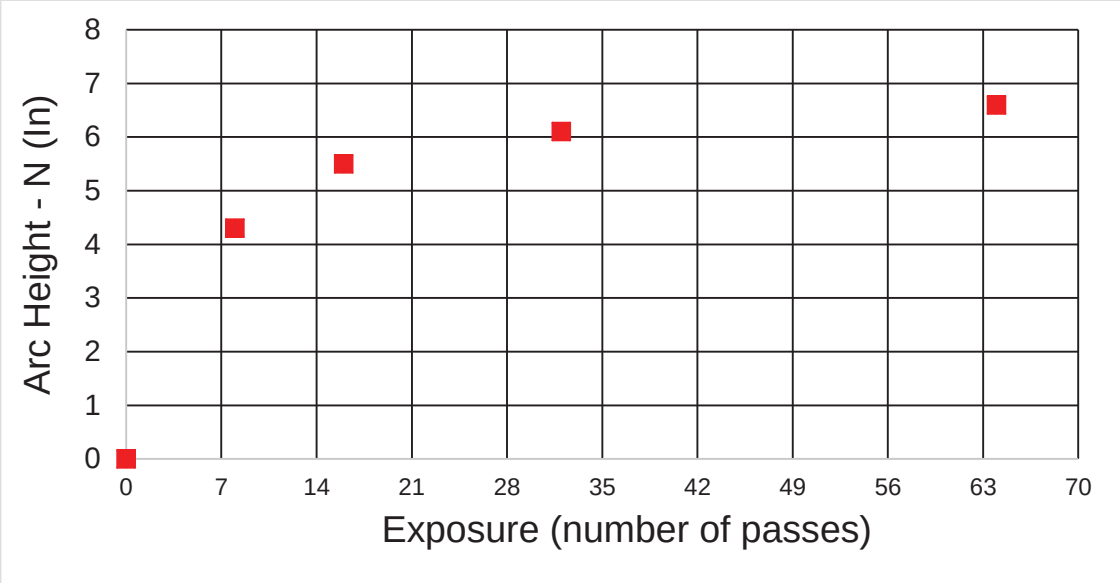

Figure 15 Results of saturation curve data from Electronics Inc. following the testing of peening parameters

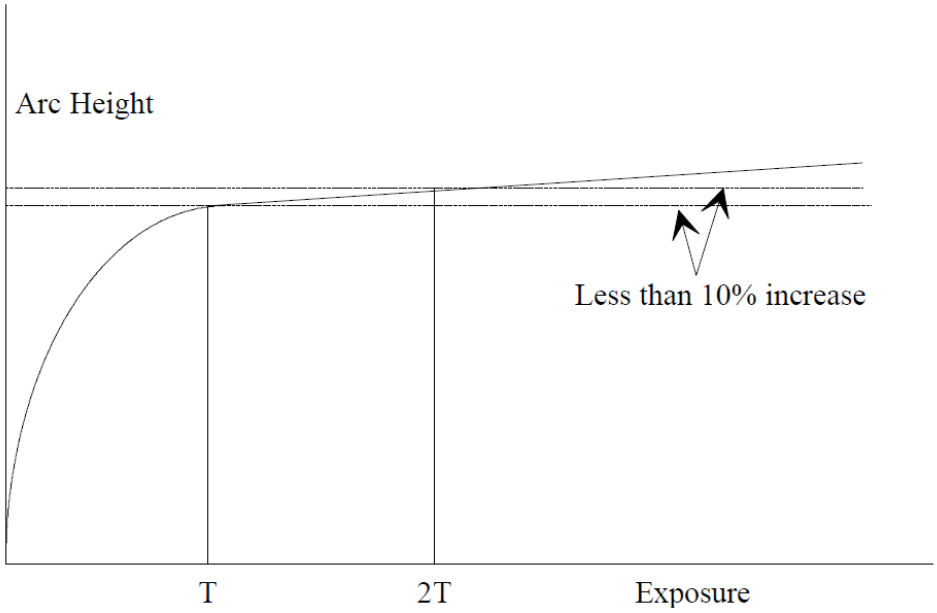

Figure 16 Graphical representation of peening saturation point, the T and 2T parameter indicative of the first point on the Almen saturation curve at which an increase of less than 10% in arc height is observed following a doubling of exposure.

Following this process, samples were visually inspected for any warping or out of plane deformation, symptoms of a significant imbalance of residual stress. All samples remained free of warping and splitting following the peening process.

3.3 Surface Preparation

Machining ‘marks’ were evident across all surfaces of the samples from the Computer Numerical Controlled (CNC) machining manufacturing process as seen in previous Figure 13. A rough surface such as this is not compatible with microstructural analysis techniques such as electron backscatter diffraction (EBSD) due to the non-uniformity of the surface geometry condition. Subsequently, a surface preparation regime was required in order to produce a uniform surface on one of each type specimen (baseline and shot peened).

3.3.1 Removing Machining Marks

Following manufacture, as previously mentioned, all samples were polished on one face to remove machining marks. This was carried out utilizing a fixed speed Buehler Ecomet V Grinder-Polisher, and a 1200 grit sand paper disc for 2 minutes under lubrication with water. However, this surface treatment still exhibited scratches and non-uniformity of the sample surface. Finer polishing techniques were required to be developed in order to successfully obtain the surface uniformity that is compatible with microstructural analysis techniques.

3.3.2 Surface Analysis

Surface roughness characterization (topography) was carried out utilizing a Zegage 3D Optical Profiler. Data acquisition was conducted by Dr. Alberto Mello. This is a non-contact, light interferometry device which was utilized for quantitative measurements of sample surface profiles. Three different surface states were analyzed for surface roughness characterization; a baseline as machined sample face, a shot peened sample face, and a sample polished for 2 minutes with 1200 grit face.

3.3.2.1 As Machined Sample Surface Face at 6.75x magnification

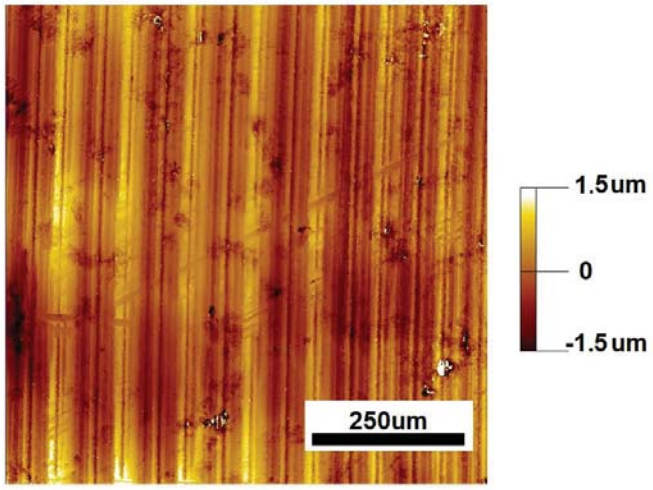

Figure 17 Top view topographic map of AA7050-T7451 following machining. CNC machining marks clearly evident.

3.3.2.2 1200 grit polished Sample Surface at 6.75x magnification.

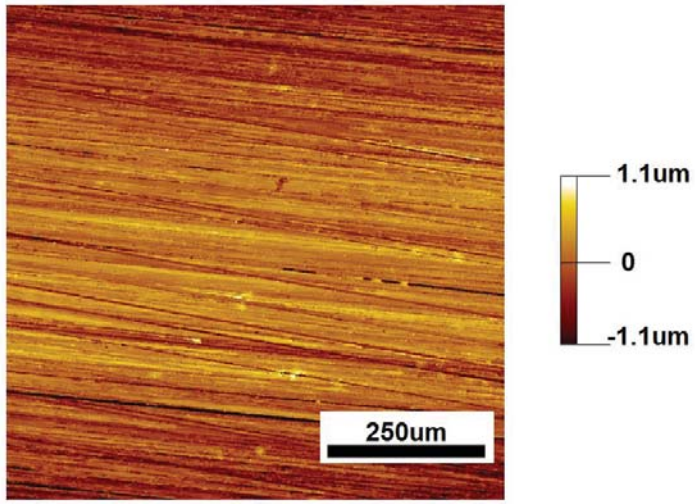

Figure 18 Top view topographic map of AA7050-T7451 following removal of machining scratches through 2 min of disc polishing with 1200 grit.

3.3.2.3 Shot Peened Sample Surface at 6.75x magnification

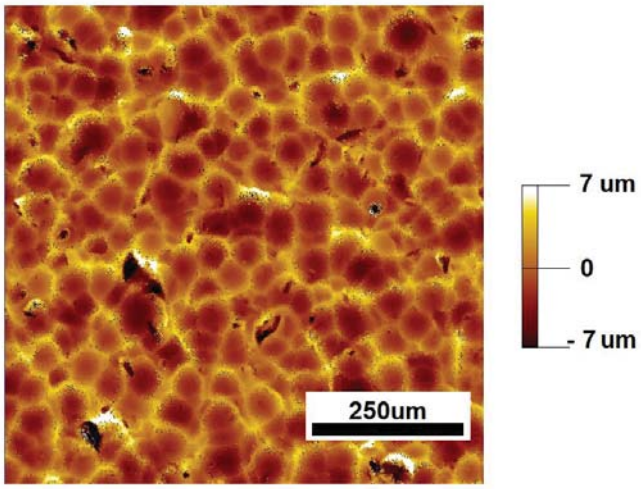

Figure 19 Top view topographic map of AA7050-T7451 following shot peening process.

The surface topography measurements were plotted to characterize a cross section of the sample surfaces, with the profile seen at Figure 20.

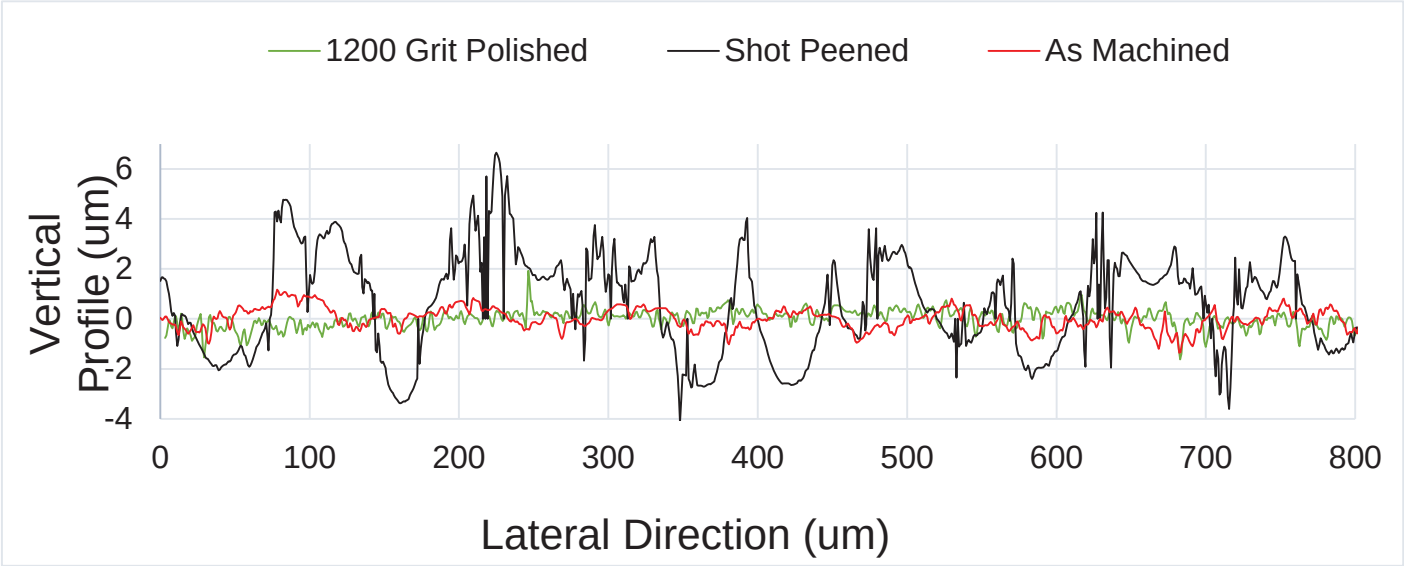

Figure 20 Comparative surface topography of the varied surface states.

3.3.3 Fine Polishing Technique Development

An experimental hand polishing regime was conducted on a sundry shot peened sample, after the shot peeing process. The intention of this was to evaluate the depth of surface roughness that would need to be removed to conduct EBSD on a uniform surface. Polishing was carried out using the Ecomet V Grinder-Polisher, and a series of short 2 minute exposures to a Pace Technologies NAPPAD 8” polishing pad loaded with distilled water and a 0.05um colloidal silica suspension. Figure 21 illustrates the removal of approximately 93um of total material over a sequence of 2 minute intervals, after each 2 minute polish an optical image was obtained using an Olympus BX51M optical microscope. The sample thickness was measured before and after the polishing process, with a Mitutoyo IP-65 Micrometer.

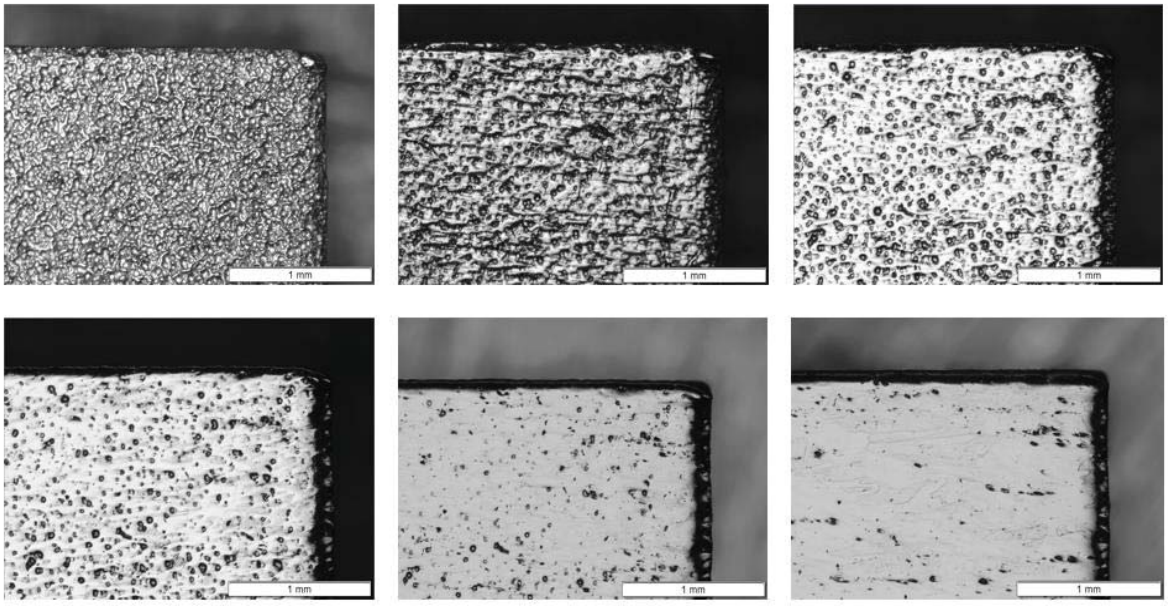

Figure 21 Incremental polishing of a shot peened sample of AA7050-T7451, demonstrating depth of surface roughness.

The polishing process uncovered the fact that approximately 90um of material was required to be removed, prior to the exposure of a completely uniform surface free of any shot peening evidence. This was interesting given the surface topography suggested the bottom of the open peening craters were at a depth of approximately 10um from the surface peaks. This is explained by the fact that the topography is a 'line of sight' technique, and not penetrating to recognize any subsurface defects. Once a uniform surface was achieved, micro-scratches which were still evident needed to be removed. Initially, it was thought that further polishing with the colloidal silica would result in a flat, uniform surface, capable of producing EBSD results, however this was not the case for two reasons. Firstly, with over polishing, chemical etching would occur, with the result shown in the Figure 22.

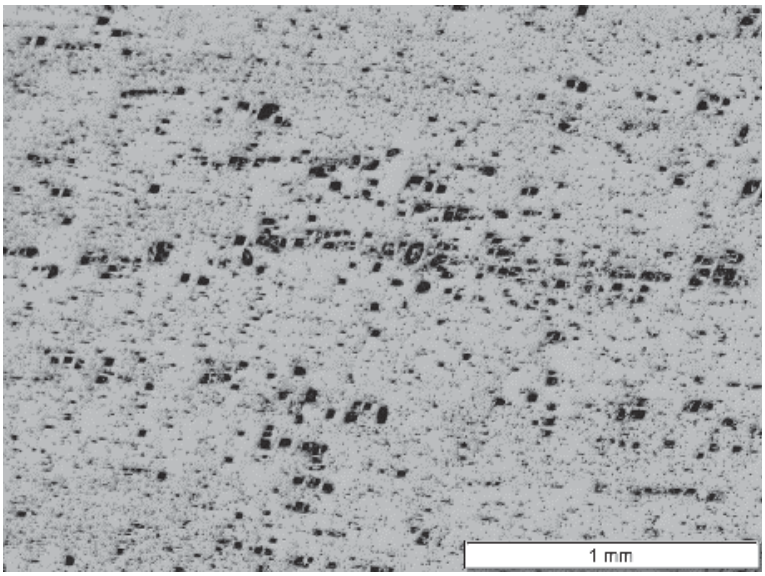

Figure 22 Chemical etching of AA7050-T7451 following extended mechanical and chemical exposure with 0.05um colloidal silica suspension.

Secondly, if 0.05um colloidal silica polishing with the NAPPAD 8" polishing pad occurred over a period greater than approximately 45 minutes, a 'mountain range' effect was observed. This effect is attributed to the hardness differential between the AA7050-T7451 matrix and the precipitate particles, with the softer matrix being polished away, exposing the harder mountainous precipitates. This effect can be observed in the Figure 23.

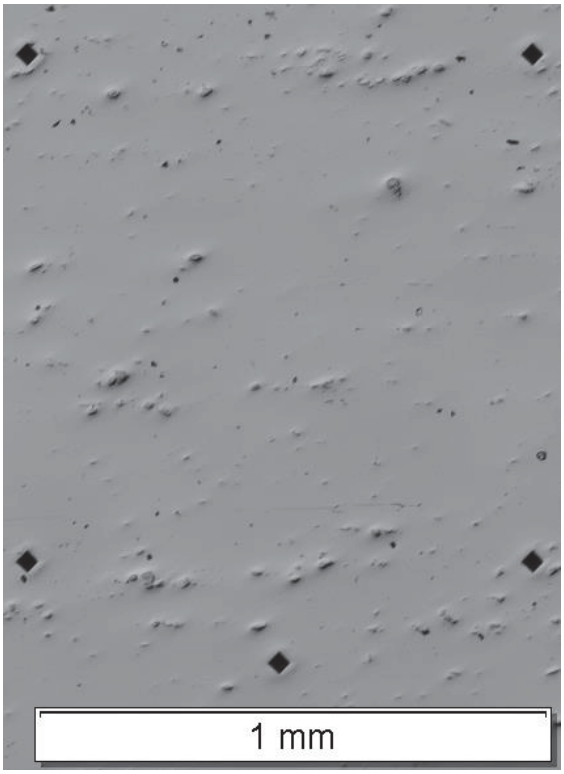

Figure 23 Mountain range effect of over polishing, exposing harder precipitates and a non-uniform substrate matrix.

Finally, these issues were resolved through a polishing process consisting of a simple 1200 grit sand paper 'cut' for 2 minutes with distilled water lubrication, effectively 'leveling' the surface, then a 40 minute fine polish using the 0.05um colloidal silica and an excess of distilled water, until a uniform, flat, and mirror like surface was achieved.

3.4 Fiducially Marking Samples

In order to secure a consistent point of reference upon the samples, fiducial markers were employed. Following polishing, and prior to the final cleaning of the samples before EBSD, a Vickers Leco micro hardness tester LM247AT was utilized to place indents marking five square areas of interest upon the polished sample surface. The indents were placed to mark up five (for redundancy in case of defects) square 1000x1000um areas upon the gauge surface of the specimen. The indents were formed using a loading at 200 grams of indentation force. Each area was marked with a label indent, following dice numbering convention, for ease of identification. The pattern was programmed using Cartesian coordinates, to give the layout seen at Figure 24.

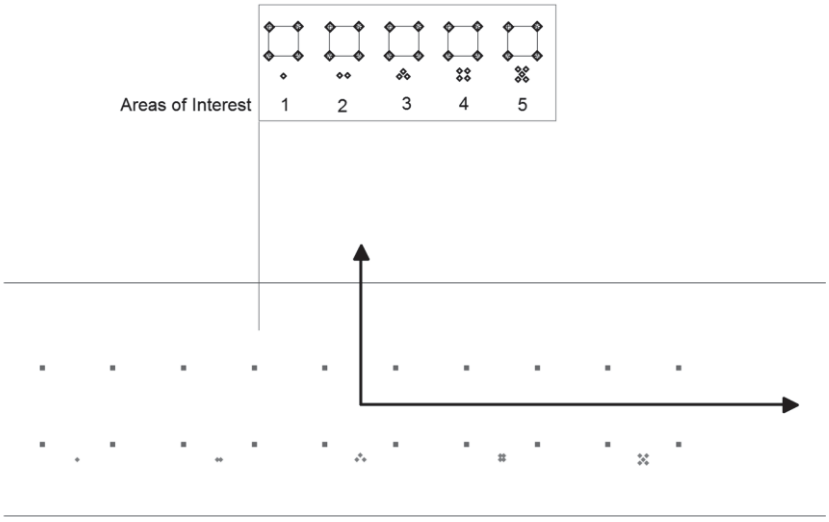

Figure 24 Fiducial markup of five areas of interest (1000x100um) upon the sample gauge section, and labelling convention.

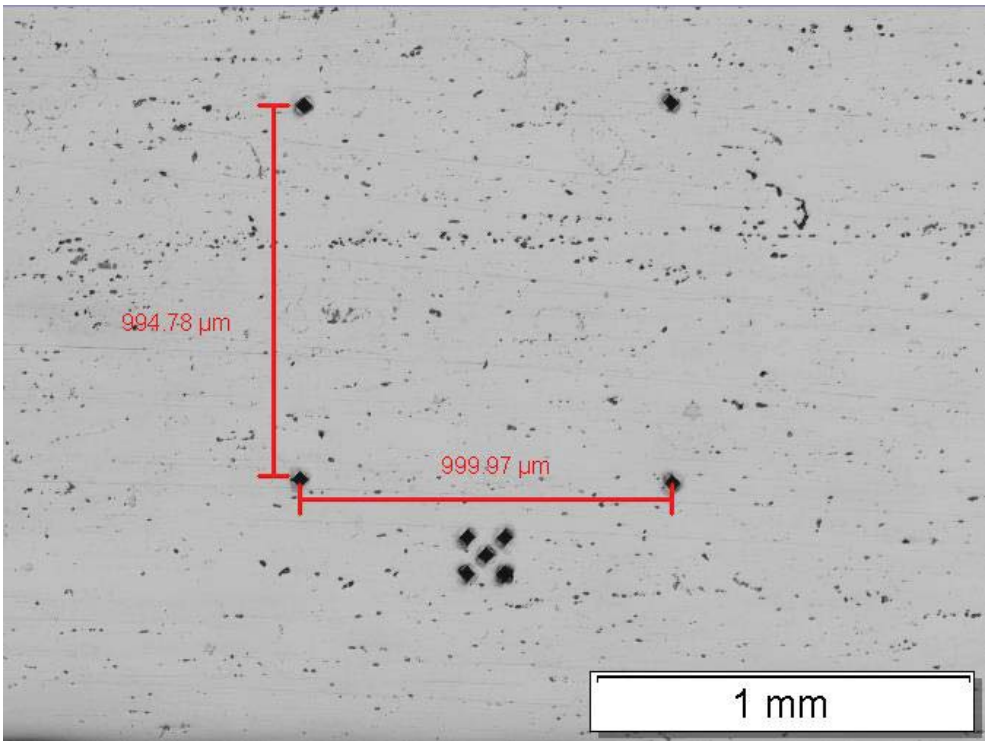

Figure 25 Fiducial markup of an area of interest upon sample.

Following the creation of this uniform surface, and reference points, microstructural analysis could commence through EBSD.

CHAPTER 4.

4.1 Electron Backscatter Diffraction

4.1.1 Background

Electron Backscatter Diffraction is a microstructural analysis technique utilized for obtaining significant amounts of data and information on the crystalline structure of the analyzed material. EBSD utilizes the combination of a scanning electron microscope (SEM), a high speed camera, and processing software in order to analyze a material. The EBSD technique is based upon diffracted electron patterns, known as Kikuchi patterns, which are generated by the constructive interference of electrons diffracted from the surface of the analyzed material, in order to determine grain orientation, texturing, and phase information. The theory of the technique is based upon the Bragg equation:

$$n\,\lambda = 2d\,sin\theta$$

According to Winkelmann *et al,*[39] EBSD systems utilize the theory of 'the Bragg equation to predict the positions of the Kikuchi band edges, and the kinematic diffraction model to estimate the relative intensities of the Kikuchi bands.' The patterns are collected using a high speed camera. The angles between the corresponding planes are cross referenced with a database of material inter-planar angles, stored within the orientation imaging microscopy (OIM) software, in order to determine microstructural makeup of the analyzed material.

4.1.2 Experimental Setup

The setup for this experimentation involved a FEI Philips XL-40 scanning electron microscope, an EBSD high speed camera, and phosphor screen. The sample orientation was placed upon a 45 degree stub, and then a stage tilt of 25 degrees was employed in order to give a total of 70 degrees (from horizontal) of sample tilt relative to the normal of the incident electron beam. An accelerating voltage of 25kV, and a spot size of 5 was utilized for the electron source. The aperture setting was 100um.

The sample mounting processes included significant surface preparation, as the EBSD technique is extremely sensitive to sample surface condition. Following the surface preparation techniques developed to give uniform surface, the samples were cleaned (chemical ultra-sonic cleaning carried out with 3 minute cleanses in each of isopropyl alcohol, acetone, and finally methanol followed by a pneumatic rinse) then mounted onto the 45 degree aluminum stub using double sided carbon tape, and copper tape for grounding and security. The sample stub assembly was then mounted on the stage within the SEM chamber, the chamber vented to vacuum, and the area of interest was identified upon the sample surface. The SEM image was acquired, focusing upon the central third of the 1000x1000um area of interest. A working distance of 17-18mm was used to focus the image, (calibrated for operation at 16-22mm) from a stage Z position of 10mm, the image was then exported to the OIM data collection terminal for selection of the scan area.

The high speed camera then relayed the diffracted electron interference patterns to the OIM data collection terminal, in which the captured image can be modified using a number of processing parameters. These include gain, black, exposure time, and an initial subtraction of background interference (noise capturing and removal). Once these parameters were optimized, a scan of the respective areas of interest was carried out utilizing a step size

conducive to a resolution appropriate for the grain size. Previous studies by Mello et al, had suggested an average grain size for the AA7050-T7541 material of 80um, subsequently, a step size for EBSD scan of 4um was selected, to give a balance of resolution and practical scan time. Parameters selected within the OIM Data Collection software included the elemental phase, of which aluminum was selected from the software's library. The Hough selected, was based on the cubic crystallographic orientation of aluminum having seven peaks.

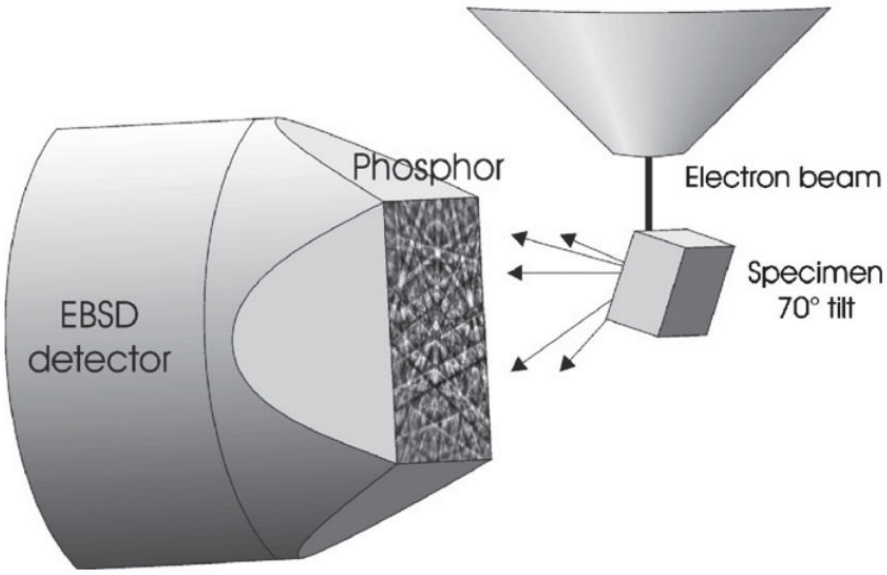

Figure 26 Schematic illustrating the experimental setup of the EBSD process within the SEM chamber.[40]

4.1.3 Results

A total of four successful EBSD scans were conducted. Two scans were carried out upon a baseline sample, and two scans were carried out upon a shot peened sample for the purposes of microstructural analysis and grain characterization. The inverse pole figure (IPF) plots of the respective sample types can be seen at Figures 27 through 30.

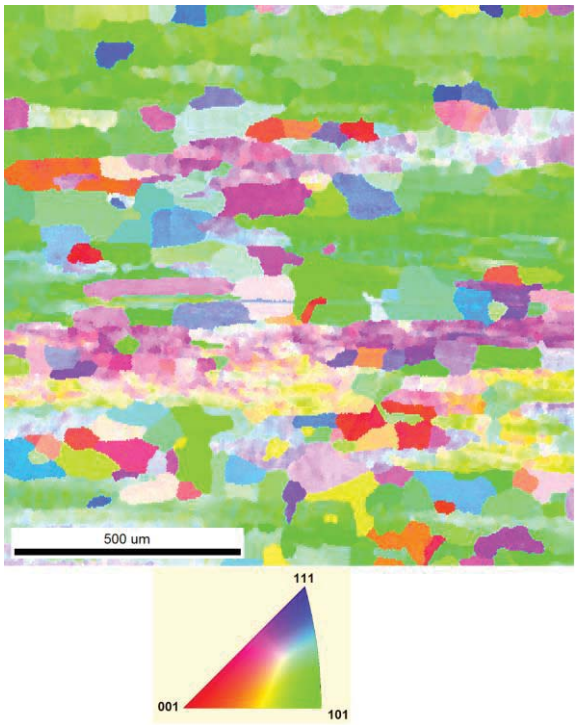

Figure 27 Shot peened inverse pole figure plot, area of interest #2, following cleaning.

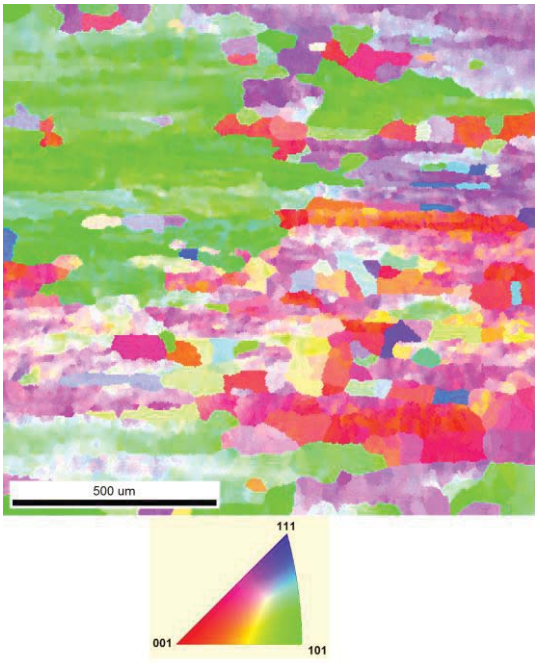

Figure 28 Shot peened inverse pole figure plot, area of interest #4, following cleaning.

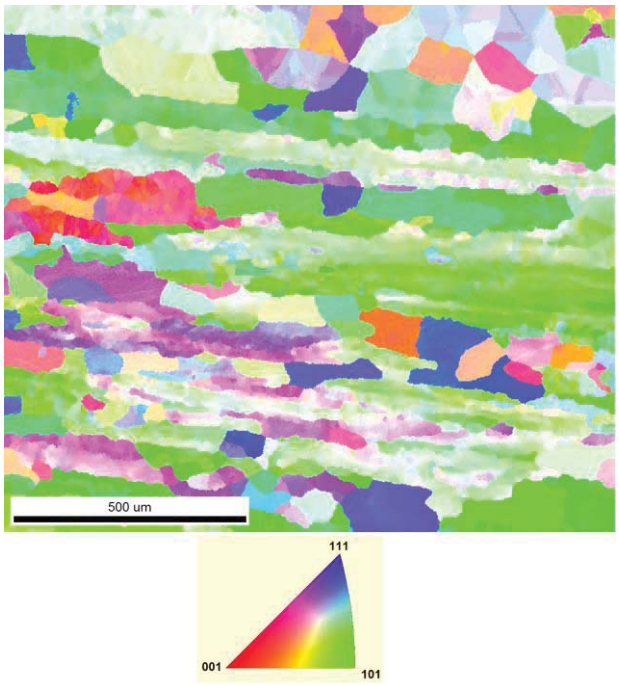

Figure 29 Baseline inverse pole figure plot, area of interest #2, following cleaning.

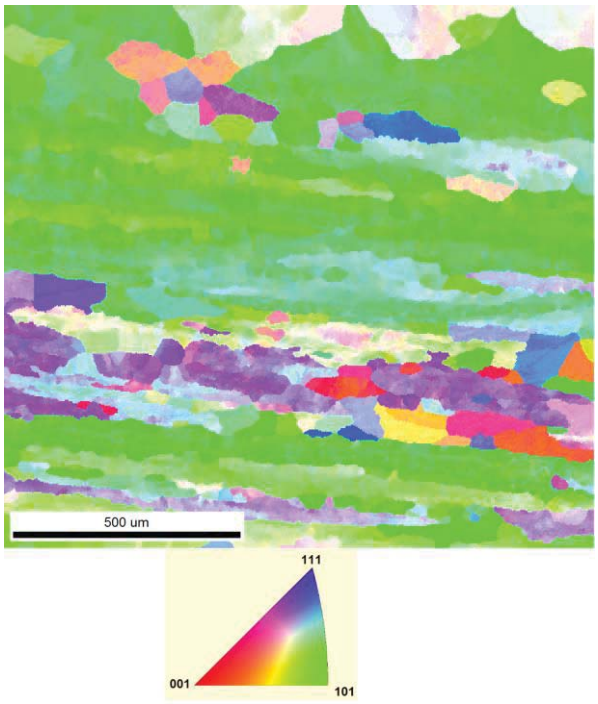

Figure 30 Baseline inverse pole figure plot, area of interest #4, following cleaning.

Table 6 EBSD scan data results summarizing scan confidence indexes and average grain geometries, *average grain geometries exclude edge grains.

Sample	Area of Interest	Average Confidence Index	*Average Grain Dia (um)	*Average Grain Area (um2)	Number of Grains	Number of Edge Grains
Baseline	2 Cleaned	0.79	62.43	3061.12	208	50
Baseline	4 Cleaned	0.84	61.14	2936.20	123	32
Shotpeened	2 Cleaned	0.94	64.04	3220.79	232	58
Shotpeened	4 Cleaned	0.94	65.26	3344.76	187	40

4.1.4 Confidence Index

In order to have what is deemed reliable data, an average confidence index (CI) of >0.10 is required.[41] The CI result is dependent upon the OIM software crystallographic orientation solutions being fitted to the Kikuchi bands, using a fitment confidence algorithm. CI ranges from 0 through to 1, and is allocated to each sampled point of the scan. All scans had acceptable average CI, above 0.10, thus qualifying as ‘reliable data’.

4.1.5 Cleanup of Data

Following the initial data collection, a consistent cleanup regime was employed to all scan results on the OIM Analysis software, in order to remove what was considered noise. Noise is caused by poor surface condition affecting the diffracted electrons trajectory, making identification and fitting of patterns impossible or inaccurate (having a low CI) in that location. Additionally, the presence of the secondary phase (precipitates) is not accounted for during the EBSD process, as the material is considered to be pure homogenous aluminum for analysis. The cleanup process involved removal of data points with CI less than 0.05, and filtering and removal of disparate, isolated, and very small orientations utilizing the OIM Analysis Software Version 6.1 post processing functions. This process

produces a representation of the microstructure considered more accurate than the originally obtained data. The following steps were carried out for all data sets during the cleaning process:

Table 7 Cleaning procedure utilized for post processing of EBSD scan data.

1:	Dilation: (tolerance 3.0, min size 30, Multi Row 1, Single Iteration 0)
2:	Grain CI Standardization (tolerance 3.0, min size 30, Multi Row 1)
3:	Grain Fit Standardization (tolerance 3.0, min size 30, Multi Row 1)
4:	Neighbor CI Correlation: (min CI 0.05)
5:	Neighbor Orientation Correlation: (level 2, tolerance 3.0, min CI 0.05)
6:	Neighbor Phase Correlation: (min CI 0.05, Singe Iteration 0)

4.1.6 Grain Orientation Distribution

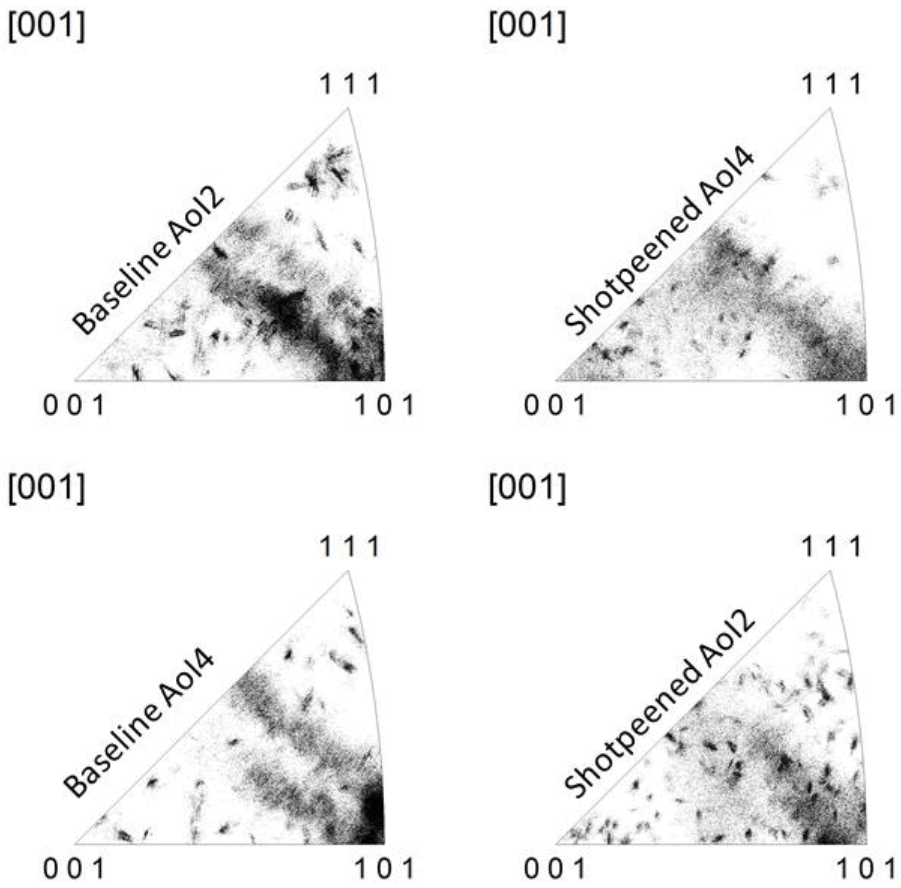

Figure 31 Stereographic triangle illustrating grain orientation distribution of baseline and shot peened scans

The stereographic triangle illustrating grain orientation distributions, shows the orientation of each of the scanned areas of interest. It should be noted there exist a banding of grain orientation in the baseline cases, with this orientation attributable to the rolling manufacturing process. The banding effect is less profound in the shot peened scans, with more randomized orientation, spreading out to the <001> orientation.

4.1.7 Grain Size Distribution

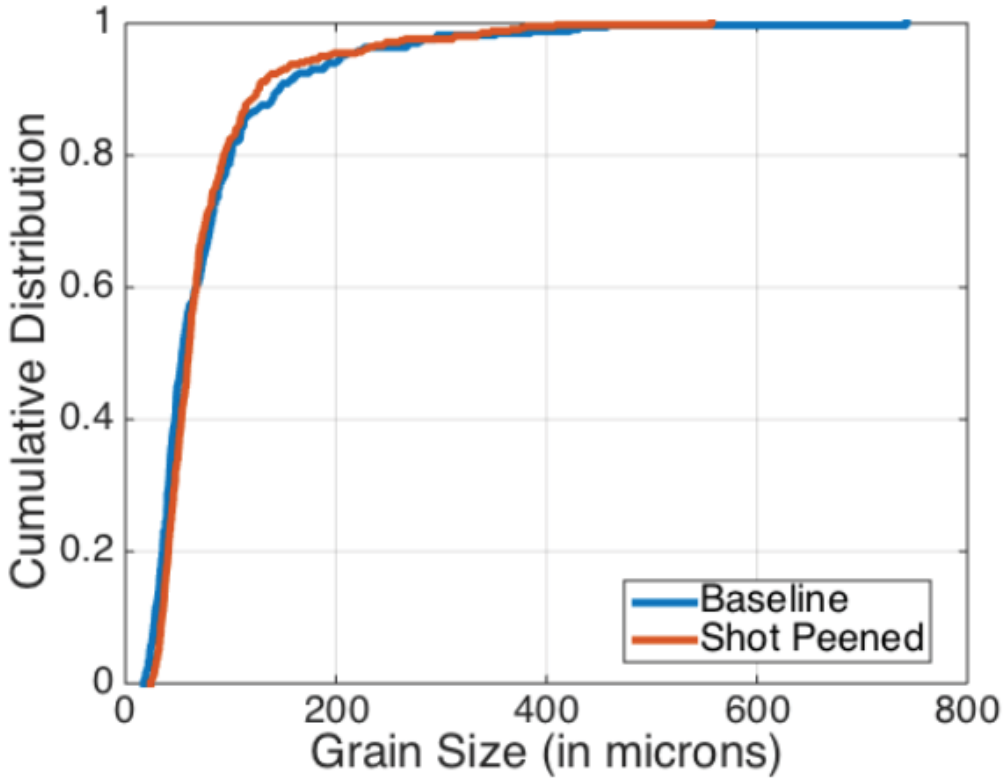

Figure 32 Cumulative Distribution of Grain Diameter.

Grain size (diameter) between the shot peened and baseline samples illustrate a relatively similar makeup. A null hypothesis test was carried out in order to discern any significance between the two sets, in terms of a difference in average grain sizing. Due to the large variance of grain size, and relative proximity of the means of the two sample sets, there is no statistical difference in average grain size for the analyzed areas of the baseline versus shot peened samples, at any reasonable level of statistical significance.

4.1.8 Grain Refinement due to Shot Peening

It is understood within literature, that shot peening has a profound effect upon grain structure, including grain refinement. At the surface following shot peening, we see severe plastic deformation caused by the process. Experimentation by Harada, *et al*,[42] explores

near surface grain refinement analysis with temperature dependency. It is shown that for higher temperatures (particularly above recrystallization temperature), the plastic deformation caused by shot peening results in significant near surface grain refinement.

This grain refinement effect is not evident within observed results. This is attributable to the polishing process and orientation carried out prior to EBSD scans on shot peened samples, the area in which grain refinement would be observed is removed when polishing to expose a sub-peening surface to approximately 90um. To observe any grain refinement in the near shot peened surface, a cross section could be taken, and polished, to evaluate the effect of peening upon near surface grain refinement, however, when polishing upon the peening face, the material providing this evidence is removed.

4.1.9 Analysis of Microstructural Attributes

Following the cleaning process, the microstructure of both the baseline and shot peened cases were analyzed. It is evident from the inverse pole figure plots, that both cases demonstrate significant grain elongation and texturing parallel to the L-T direction. This microstructural characteristic is attributable to the manufacturing process, is which the rolled plate was produced, with the rolling direction in the L-T. Subsequently, we see evidence of grain elongation in this direction. This type of textured grain structure can contribute to anisotropic directional properties, however the effect is considered consistent between the baseline and shot peened cases, and is dismissed for the purposes of this research. For each of the baseline and shot peened sample scans, we observe an average grain diameter of approximately 60-65um.

4.1.10 Energy Dispersive (X-ray) Spectroscopy - Background

In order to conduct elemental analysis upon the samples, a technique of energy dispersive x-ray spectroscopy was utilized. This was carried out using a FEI Philips XL-40 scanning electron microscope. EDS utilizes x-rays generated by the interaction between the beam and the analyzed specimen interaction, in order to evaluate elemental composition. According to the FEI Philips XL-40 SEM Elemental Analysis user guide, 'x-rays are generated up to a few micro-meters deep into the specimen (shallower for high Z elements and deeper for low Z elements, and for an area of 0.2um in diameter on the surface.'[43] In order to stimulate the release of an elementally unique x-ray, EDS relies upon a high energy beam (in this case an electron beam) to be focused onto the subject sample. This high energy beam excites the analyzed element's indigenous electron to jump to an alternate shell during which it emits unique x-rays (which can be measured via a spectrometer). Since the unique x-rays correspond to an energy level associated with a specific jump in atomic shells of an atomic element, this can be cross referenced to determine what the elemental makeup of the analyzed sample's constituents.

4.1.11 Experimental Setup

Elemental analysis was conducted on a polished sample of AA7050-T7451. The sample was prepared under the same conditions as EBSD, in the polished state, with chemical ultra-sonic cleaning carried out with 3 minute cleanses in each of isopropyl alcohol, acetone, and finally methanol, in addition to a pneumatic rinse. The sample was then mounted onto a flat aluminum stub, using double sided carbon tape, and copper tape for grounding and security. The sample stub assembly was then mounted upon the stage in the SEM chamber, the chamber vented to vacuum, and the area of interest was identified upon the sample surface. The SEM image was acquired using a Z stage of 10mm, working

distance of 16-17mm, beam energy setting of 25kV, and spot size 5, focusing upon a precipitate particle, which was then exported to the EDAX Genesis microanalysis data collection terminal. A dwell point was analyzed, both on the identified precipitate, and on the matrix itself in order to evaluate the chemical constituents of each region.

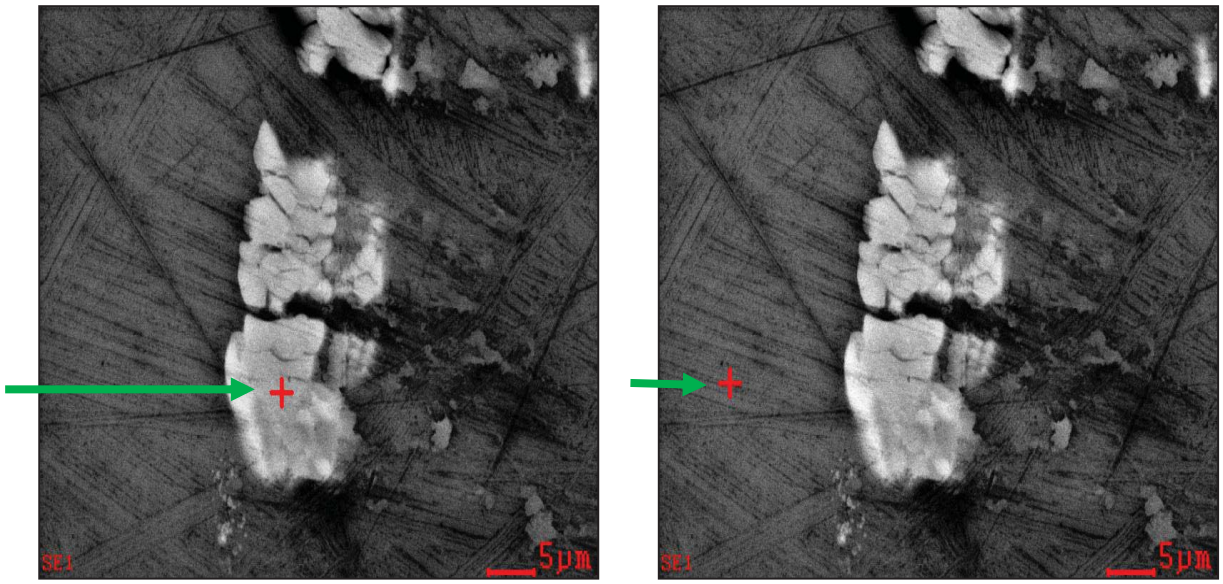

Figure 33 Dwell points selected via the cross hair, for elemental analysis, (Left) interrogating the precipitate, and (Right) interrogating the material matrix

4.1.12 Results

Results of the elemental analysis showed that following at least 500 counts, the chemical constituents of the precipitate interrogation included copper (Cu), iron (Fe), and aluminum (Al). The matrix material returned only aluminum (Al), as expected. Subsequently, these results correlate with the work of Mello *et al*,[44] suggesting that the precipitates are predominantly Al_7Cu_2Fe, and confirm the nature of the precipitates for further analysis involving nano-indentation and SEM imaging through interrupted fatigue. Small inconsistent returns of magnesium (Mg) were also noted.

CHAPTER 5.

5.1 Fatigue Loading

5.1.1 Fatigue Equipment

A combination of two different axial load frames were utilized in this research in order to apply fatigue load cycling to the samples. Initially, a Mark-10 ESM1500 electric screw driven load frame was employed for relatively low (<100 cycles) cycle fatigue. The Mark-10 is a single column load frame, capable of loading up to 6.7kN (1500lbF), has a travel range of 32in. (813mm), and an available cross head speed range of 0.02-2,300mm/min (0.001-90in/min). The load frame is configured with Series R01 load cell (force sensor), and Mark-10 G1061-2 Model grips.

Figure 34 Mark-10 ESM1500 load frame.

Secondly, a larger, custom built hydraulic drive MTS load frame was utilized for the higher (>100 cycles) fatigue loading. The MTS load cell consists of a model 244.12 hydraulic ram (actuator), capable of loading up to 25kN (5620lbF), in combination with an MTS 661.20E-01 load cell (transducer), capable of sensing loads of up to 25kN (5620lbF). The gripping mechanisms utilized were MTS 647 hydraulic wedge grips, capable of gripping pressure up to 21MPa.

Figure 35 MTS load frame, illustrating hydraulic grips, test frame, and grip control panel.

5.1.2 Fatigue Testing Preparation

Fatigue testing variables were selected as follows:

Table 7 Fatigue Testing Parameters

Parameter	Mark-10 Load Frame	MTS Load Frame
Maximum Stress (σ_{MAX})	400 MPa	400MPa
Minimum Stress (σ_{MIN})	20 MPa	20 MPa
Frequency/Cross Head Speed	2mm/min	3 Hz
Stress Ratio (R)	0.05	0.05
Loading Shape	Saw tooth	Sinusoidal
Gripping Mechanics	Mechanical screw drive wedge	10 MPa in hydraulic wedge

The test loading thresholds were chosen as ~85% of the material's tensile yield strength (469MPa), as the maximum stress of 400MPa, and a stress ratio of 0.05 gave a minimum stress of 20MPa. This ensured that the fatigue loading regime remained within the elastic region, given the material properties of the sample material.

5.1.2.1 Mark-10 Crosshead Speed Selection

For the Mark-10 Load Frame, a stress command versus stress measured analysis was carried out in order to assess the compliance of the machine at varying cross head speeds. With any crosshead speed greater than 3mm/min, an overshoot of stress commanded would

occur, and subsequently, to ensure stress measured replicated stress commanded, cyclic fatigue was run at 2mm/min on this load frame.

5.1.2.2 MTS Fatigue Testing Frequency Selection

For the MTS Load Frame, the cyclic frequency was also analyzed through a force command versus force measured comparison for a range of frequencies. The purpose of this evaluation was to select a test frequency with an 'acceptable'[45] delta between force commanded and force actual. In order to establish this threshold frequency, an analysis of force error was carried out at each frequency 0.67Hz through to 9Hz. Results below, show the average delta between force commanded and force actual when conducting a 400 cycle test, with a data sampling rate of 60Hz, and a maximum stress of 400 MPa, minimum stress of 20MPa. It should be noted that this test was ran from 0 to 400 cycles for each frequency, and captures the error between force command and force measured as the compensator 'ramps up' and chases the commanded force, taking approximately 80 cycles to reach the desired stress maximum and minimum for lower frequencies (less than 3Hz), and the number of cycles to equilibrate measured and commanded increasing exponentially at higher frequencies, thus increasing error. This testing was ran on a dummy sample with a cross sectional geometry of 1.26 x 3.03mm at the gauge, this translated into a set point of 801.47N and an amplitude of 725.14N to result in the desired stress parameters (400MPa and 20MPa).

Results of force commanded versus force measured (average absolute error) for a range of cyclic frequencies are shown at Figure 36.

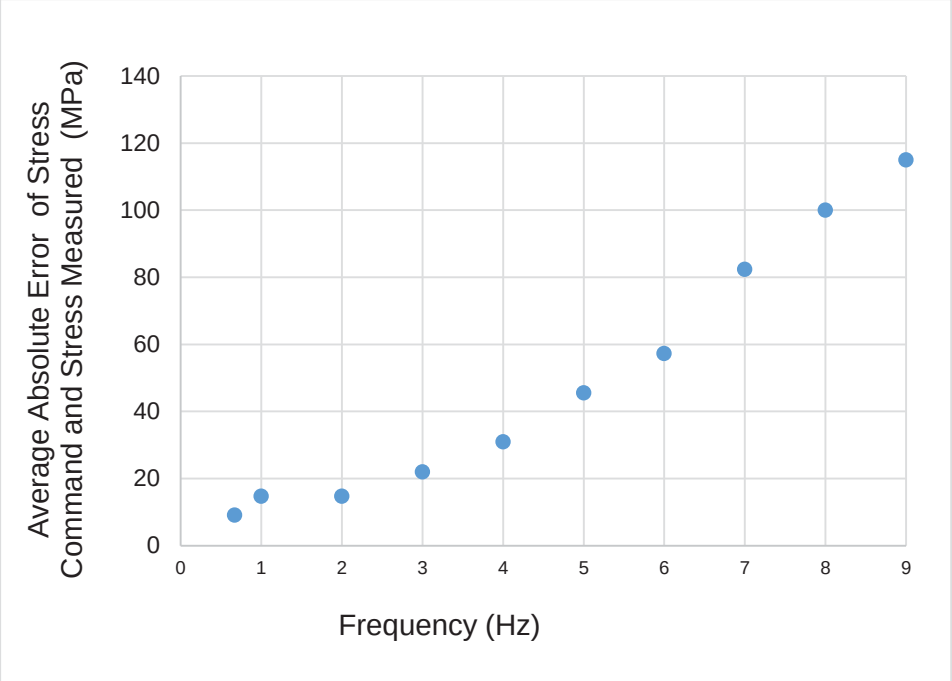

Figure 36 MTS Load Cell frequency accuracy evaluation. Average Absolute Error between measured and commanded stress over a range of frequencies.

5.1.3 Interrupted Fatigue Analysis.

Prior to fatigue testing commencement, a sample throughput sequence was draw up, for which interrupted fatigue analysis could be conducted via other experimental methods (x-ray diffraction, nano-indentation, SEM imaging) for each sample at incremental stages of fatigue.

A sequence of which would enable the iterative analysis of samples via x-ray diffraction for residual stress, at varied levels of fatigue cycling (n= 0, 1, 10, 100, 1000, 10000, and 15000) was employed. Following this staggered fatigue analysis, all samples were finally cycled until failure. The unique geometry and loading parameters resulting consistent stress controlled fatigue is listed at Table 8.

Table 8 Sample Geometry and Loading Parameters

Sample Type	Reference	Gauge Cross Sectional Area (mm^2)	Setpoint (N)	Amplitude (N)	Force MAX (N)	Force MIN (N)	Failure (cycles)
Baseline	A15	4.596	965	873	1838.488	91.9244	26543
Baseline	A11	4.444	933	844	1777.436	88.8718	21170
Baseline	A4	4.502	945	855	1800.7952	90.03976	17561
Baseline	A8	4.494	944	854	1797.614	89.8807	26921
Baseline	A14	4.489	943	853	1795.752	89.7876	25573
Shotpeened	SP1	4.665	980	886	1865.824	93.2912	14160
Shotpeened	SP2	4.628	972	879	1851.2664	92.56332	25087
Shotpeened	SP3	4.658	978	885	1863.22	93.161	23590

Loading parameters in amplitude and set point were derived from sample geometry at the gauge section measured using a Mitutoyo IP-65 Micrometer with care to ensure no stress concentrations or scratches were imparted onto the samples. Small variations in sample geometry resulted in unique loading parameters for each sample to ensure consistent stress.

Set point is the mean force, with amplitude being the alternating force.

$$Setpoint = \frac{ForceMAX + ForceMIN}{2}$$

$$Amplitude = \frac{ForceMAX - ForceMIN}{2}$$

5.1.4 Cycling through to Failure Results

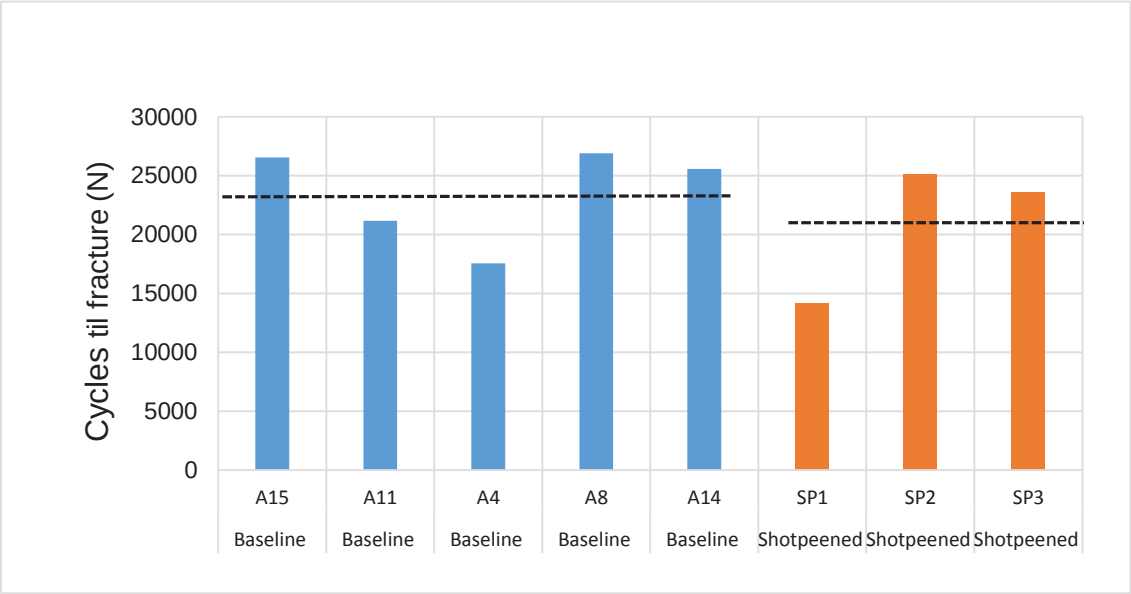

Figure 37 Results of fatigue testing until failure of AA7050-T7451 samples, baseline and shot peened.

The shot peened sample set failed after an average of almost 21,000 cycles. The baseline sample set failed after an average of almost 23,500 cycles. A statistical hypothesis test was carried out, resulting in no statistical difference in the average cycle to failure performance of the baseline versus the shot peened sample average, at any level of reasonable significance. Subsequently, with the small sample size and large variance, no significant conclusion can be drawn regarding the effect of shot peened versus baseline fatigue performance for this experimentation. However, it is stated by Lieurade and Bignonnet[46] that compressive residual stresses can only improve fatigue strength provided that there is no 'rapid relaxation of these stresses in service.' Evidence of such a rapid relaxation is provided later through x-ray diffraction results (significant reduction of compressive residual stress at approximately the 10k-15k cycle point) which may have been a contributing factor in the fatigue performance observed in the shot peened samples.

5.1.5 Stress Strain Relation through Fatigue

The stress versus strain relationship through fatigue has been plotted for various lifecycle points for both the baseline and shot peened samples. Stain measurements were taken with a MTS Model 632.26 B30 extensometer with a gauge length of 7.62mm for comparison of baseline and shot peened response. Figure 38 illustrates the relationship for both cases, in early and later fatigue points.

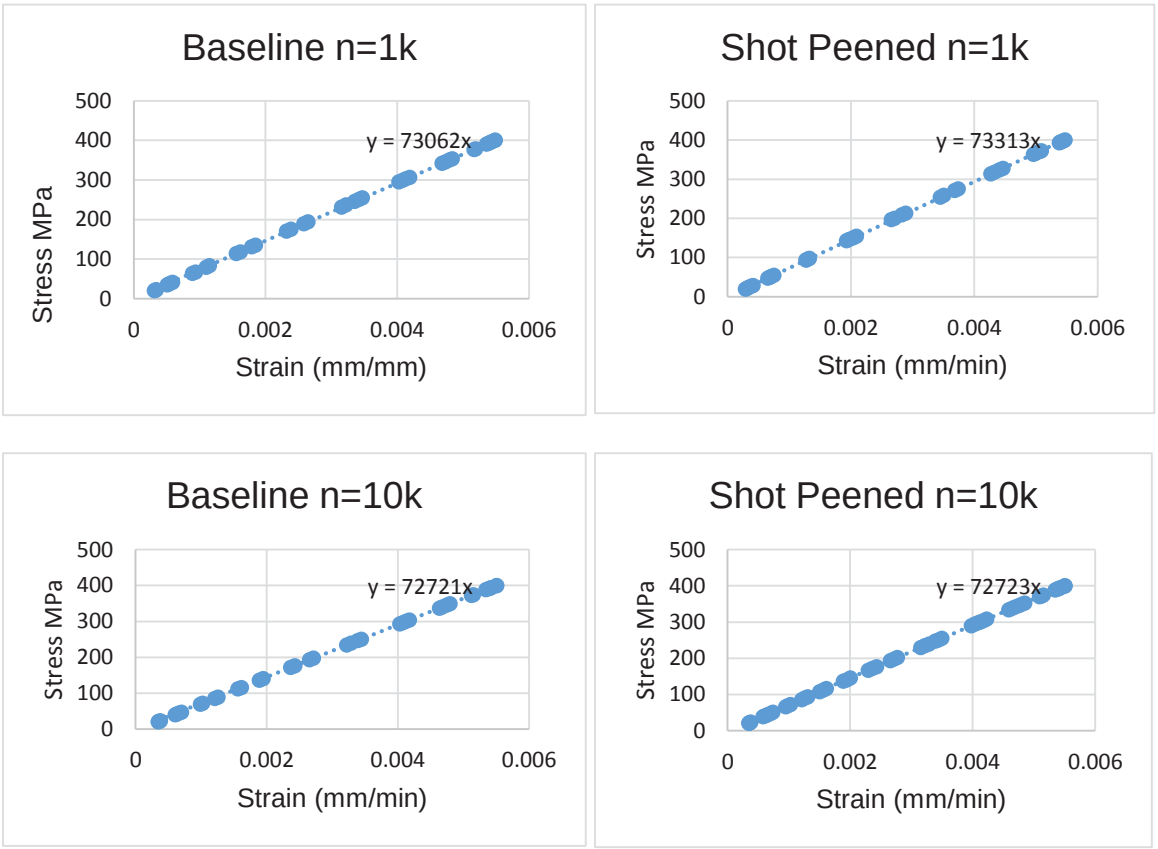

Figure 38 Stress Strain relationships for AA7050-T7451 in varied stages of fatigue, in baseline and shot peened samples. Of note, no plastic deformation leading to hysteresis loop opening, due to stress controlled loading remaining in the elastic region. Elastic modulus (linear trend line gradient) correlates with known value for AA7050 (71.7GPa).

5.2 X-Ray Diffraction

5.2.1 Background

X-ray diffraction is a common non-destructive technique in the evaluation of residual stresses in metallic polycrystalline lattice materials. The Measurement Good Practice Guide states that 'in measuring residual stress using x-ray diffraction, the strain in the crystal lattice is measured, and the associated residual stress is determined from the elastic constants assuming a liner elastic distortion of the appropriate crystal lattice plane.'[47] The number of different grains of which contribute to the measurement, is dependent upon the grain size and beam geometry. X-ray diffraction is considered to be a near surface measurement, ideal for analysis of surface treatment processes such as shot peening. Through residual stress measurements, it is possible to correlate this qualitative data with fatigue performance results, as the technique can be utilized to assess the magnitude of average compressive residual stress of near surface shot peened samples.

5.2.2 Principles

X-ray diffraction relies upon the emission of x-rays from a beam source (S), which are emitted in a narrow beam focused onto the analyzed material sample surface (in a known orientation), and then diffracted based upon the state of the polycrystalline lattice material. The diffracted x-rays are then sensed by an x-ray detector (D). The diffraction angle (2θ) is the angle between the incident beam's subsurface trajectory (should it have continued on the incident path), and the diffracted beam. The angle psi (ψ) defines the orientation of the sample, and is the angle between the incident and diffracted beam bisector, and the normal of the surface (N).

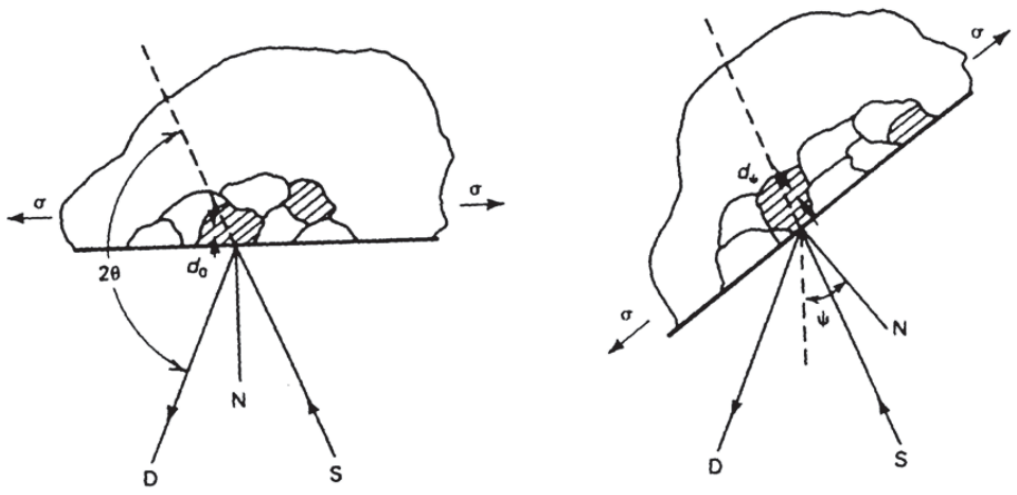

Figure 39 Schematic of x-ray diffraction's principle geometry, with (Left) sample at orientation $\psi = 0$ and (Right) orientation $\psi = \psi$. [48]

According to Bragg's Law, the diffraction angle (2θ) is dependent upon the crystalline lattice spacing of the material, d. Subsequently, any change in d, i.e. a residual stress state (due to elastic strain), results in a corresponding change to the measured diffraction angle. 'Measuring the change in in the angular position of the diffraction peak for at least two of the sample defined by the angle psi (ψ) allows the calculation of the residual stress present.'[49]

The x-ray diffraction process, subsequently can only detect changes in d associated with elastic strain, as any change in d greater than elastic will induce plastic deformation and dislocation of the material crystalline structure. Subsequently, x-ray diffraction residual stress measurements are a representation of the residual stress due to elastic strain on a macroscopic scale of which the x-ray beam is averaged over a volume. This is stated as 'the residual stress determined using x-ray diffraction is the arithmetic average stress in a volume of material define by the irradiated area which may vary from square centimeters to square millimeters, and the depth of penetration of the x-ray beam.'[50] According to literature, the shallow depth of penetration of x-rays involved with aluminum alloys

dictates that 50% of radiation is diffracted 'from a layer approximately 0.005mm deep for the radiation typically utilized for stress measurement.'[51] Additionally, 'the choice of diffraction peak selected for residual stress measurement impacts significantly impacts the precision of the method, the higher the diffraction angle, the greater the precision.'[52]

5.2.3 Residual Stress Calculation: the $\sin^2\psi$ technique

Software utilized in this research utilizes the $\sin^2\psi$ technique of residual stress calculation. This technique involves the linear regression trend line fitting (slope of best fit) to multiple psi (ψ) angle measurements, from which a 'stressed' lattice spacing average is derived, d_ϕ, and then subsequently utilized in the following equation to generate a residual stress value:

$$\sigma\phi = \left(\frac{E}{1+v}\right)_{(hkl)} \frac{1}{d_{\phi 0}} \left(\frac{\delta d_{\phi\psi}}{\delta sin^2\psi}\right)$$

5.2.4 Experimental Setup

All x-ray diffraction experimentation was carried out at the Frederick Seitz Materials Research Laboratory Central Research Facilities, University of Illinois. The experimental setup was kindly configured by Dr. Mauro Sardela, Head of the University of Illinois Materials Research Laboratory. Sample preparation for x-ray diffraction involved mounting samples upon glass microscopic analysis slides, taped together using 3M adhesive tape, and the assembly of samples on the slides were mounted upon the stage. The positions of the area of analysis for each sample was then input into the control software via Cartesian coordinate system point of reference.

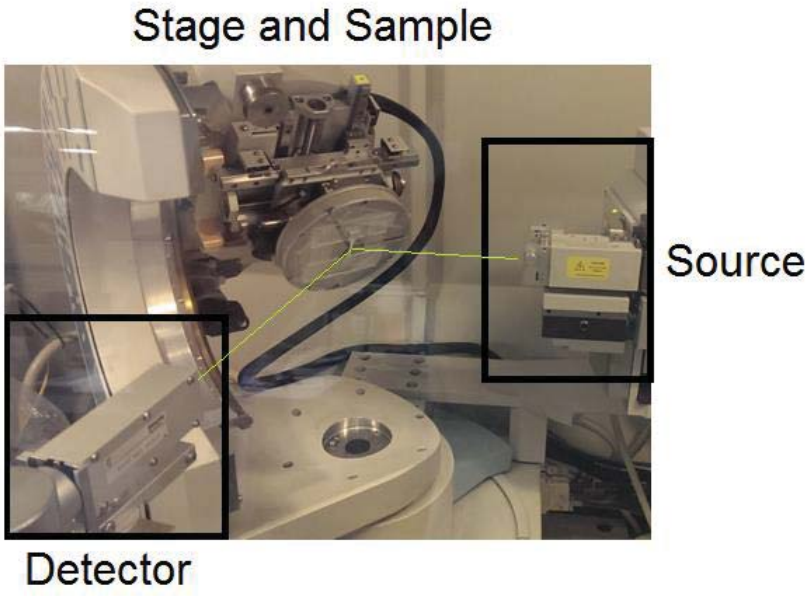

Figure 40 X-ray diffraction experimental setup showing x-ray source, stage mounted sample, and x-ray detector.

The experimentation utilized the ‘X’Pert 2’ x-ray diffraction system. The system comprised of a Cu point focus x-ray source, primary optics of x-ray lens, secondary optics of anti-scatter slits, a radiation wavelength of 0.15418nm (Cu K alpha 1 and K alpha 2), and a PIXcel point detector. X-ray generator voltage was 40kV. The data software utilized was ‘X’Pert Data Collector’, utilized for both instrument control, and data acquisition. For each sample, a peak scan was ran, in order to generate a diffraction peak profile. All samples were AA7050-T7451, with individual diffraction peak profiles ran for each measured sample.

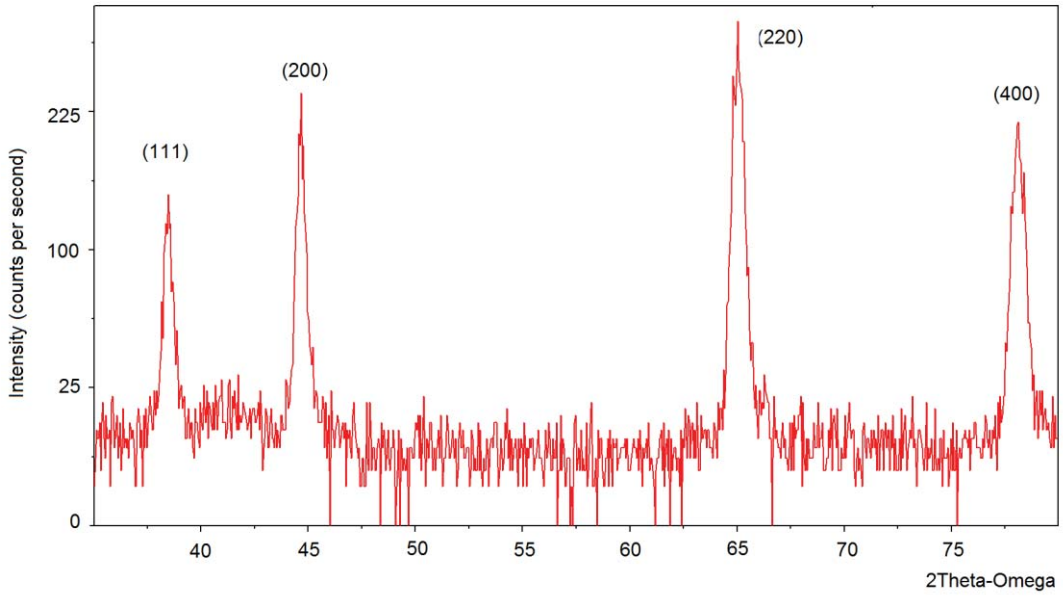

Figure 41 A diffraction peak profile for AA7050-T7451 illustrating peaks and associated Miller indexes.

For all scans, the [4,0,0] Miller index peak was utilized for residual stress determination, as this is the highest 2θ peak in the profile, giving greatest measurement precision.

5.2.5 Measurements Conducted

Residual stress measurements were conducted upon the front and rear face of shot peened samples, at the aforementioned seven stages of fatigue (n= 0, 1, 10, 100, 1000, 10000, and 15000). This yielded a total of 14 results for the shot peened samples. For the baseline samples, three measurements were carried out at varied stages of fatigue (n=0, 100, 10000).

5.2.6 Residual Stress Results

Table 9 exhibits residual stress measurement results determined via x-ray diffraction.

Table 9 X-ray diffraction results of interrupted fatigue.

		Front of Sample		Rear of Sample	
Sample Condition	**Fatigue Cycles (n)**	**Residual Stress Result (MPa)**	**Error**	**Residual Stress Result (MPa)**	**Error**
Shot Peened	0	-246.7	21.6	-194.6	13.7
Shot Peened	1	-248.9	10	-268.2	18.3
Shot Peened	10	-229.4	22.7	-234.9	18.3
Shot Peened	100	-222.6	17.6	-267.6	16.5
Shot Peened	1000	-214.3	18.5	-245.8	11.3
Shot Peened	10000	-217.5	16.2	-216.6	17.7
Shot Peened	15000	-147.7	18.1	-147.2	13.8
Baseline	0	-5.7	16.5		
Baseline	100	-28.4	17.7		
Baseline	10000	-49.6	24.2		

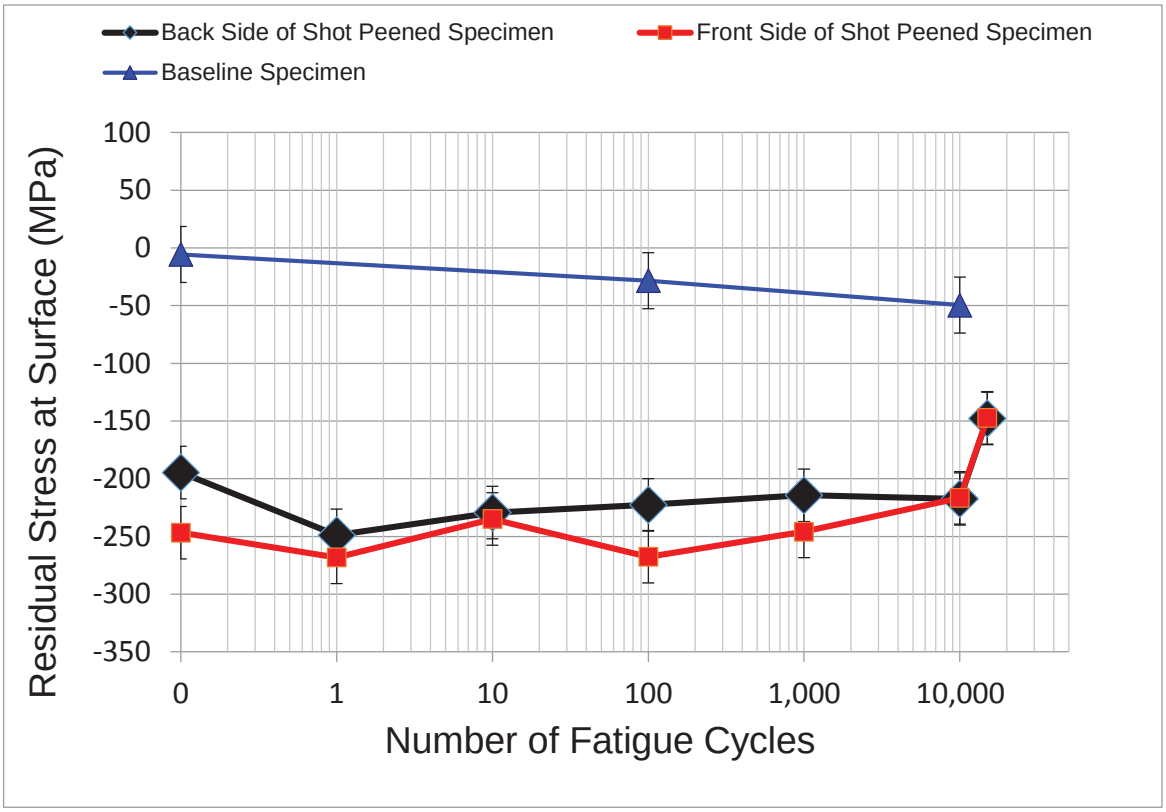

Figure 42 X-Ray Diffraction – Residual Stress at Surface Measurements

5.2.7 Discussion

Following the fatiguing of samples, and intermittent x-ray diffraction residual stress measurements, we see some interesting results. Notably, there is a consistent differential in the compressive residual stress between the front and back face of the samples. This result may be attributable to one of the following factors; firstly, the staged shot peening process, by which one face of the dog bone specimen is peened, then the specimen is turned for peening on the opposite side, may result in an asymmetry due to the order of work being done by the peening process, with the initial peening having a cold working effect through the thickness of the thin specimen. Secondly, the condition of each surface (one side as CNC machined, and the other in the 1200 grit finish) when the samples were sent to be

peened may have an effect on the resultant residual stress, as Sharpe and Clarke[53] suggest that the surface roughness can significantly contribute to the residual stress magnitude.

Secondarily, we note an asymmetric relaxation between the two surface faces of the compressive residual stress magnitude through fatigue cycling for the shot peened samples. Qualitatively, we see the higher absolute magnitude residual stress face relax earlier in fatigue than the lower absolute magnitude residual stress face. At the 10,000 cycle point, we also observe an equilibrium of compressive residual stress, and then a rapid symmetric relaxation through to the 15,000 cycle point.

With regards to the baseline result, we note a slight deviation through fatigue towards a compressive state. However, this is considered insignificant, and deemed to be within the realm of measurement error. The baseline sample type remains in a relatively stress free state throughout fatigue.

5.2.8 Residual Stress Profile from Nano-Indentation

The following element of this research was carried out in co-operation with Siavash Ghanbari, under the supervision of Prof. Bahr, and the Materials Engineering Department's Center for Surface Engineering and Enhancement.

5.2.8.1 Principle of Residual Stress Measurement by Nano-Indentation

An experimental methodology of determining through thickness residual stress profiles of a cross sectioned shot peened sample has been carried out. This has been undertaken via nano-indentation. This was carried out based upon the Suresh and Giannakopoulos model.[54] The nano-indentation procedure was undertaken utilizing a Hysitron TI950 TribIndenter, in conjunction with a Berkovich pyramid indentation tip. The indentation procedure involves the penetration of a flat, uniform surface of the analyzed substrate with

the indentation tip. Whilst the indentation occurs, the measurement instrumentation records the applied force, P, and the indentation depth, h. This data is continuously logged during the process. Suresh and Giannakopoulos have developed a method of estimation of near surface residual stress, based on numerous assumptions, utilizing the aforementioned data.[55] This model is founded upon Kick's law:

$$P = Ch^2$$

Whereby, C is a measure of the curvature of the loading ramp of the load depth (P-h) curve, which signifies loading compliance.

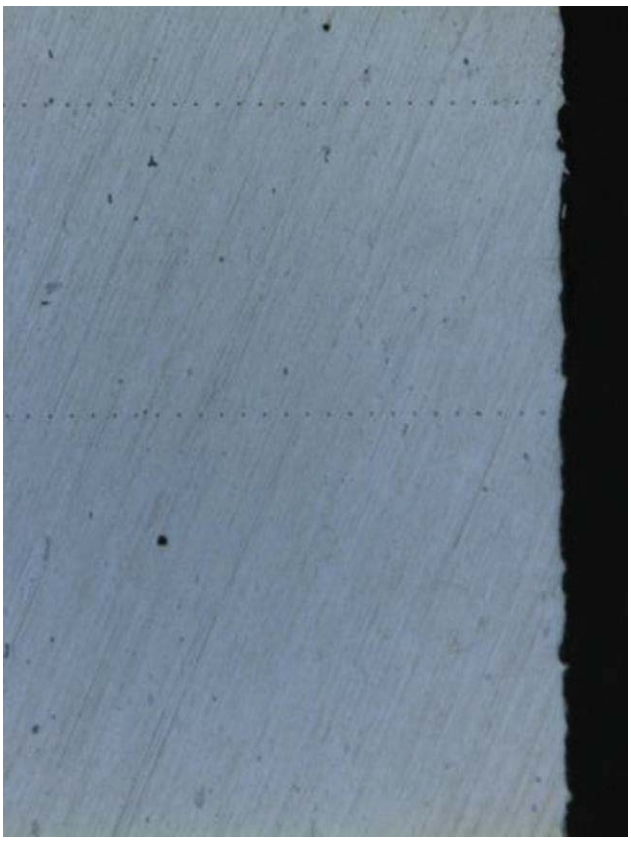

Figure 43 Cross section of shot peened AA7050-T7451 with nano-indentation through the 1.6mm gauge thickness, showing nano-indent measurements across the sectioned gauge at a spacing of 10um.

5.2.8.2 Qualitative Results

It should be noted that the following through thickness residual stress profile was scaled, in order to comply with the equilibrium condition (through thickness stress balance of tension and compression).

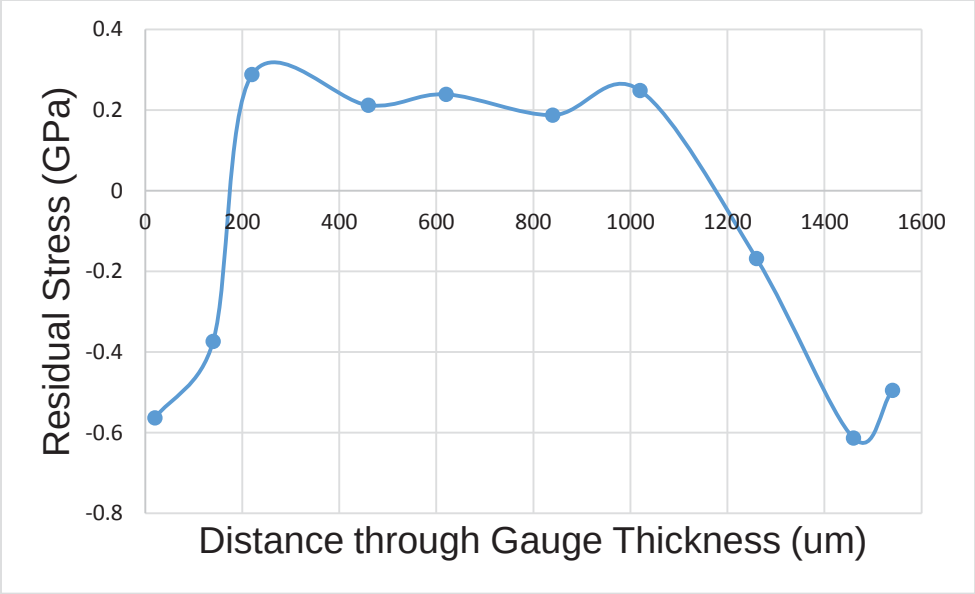

Figure 44 Through thickness (1.6mm) residual stress profile of shot peened AA7050-T7451 derived from nano-indentation force depth results, and Suresh and Giannakopoulos residual stress model.

Whilst the experimental model of Suresh and Giannakopoulos does not produce precise quantitate results in this case in terms of precision through thickness residual stress magnitude measurement, from a qualitative perspective, we can see that the resultant residual stress profile is in agreement with the trend expected from literature and more precise experimental evidence. A compressive region of residual stress extends to a depth of approximately 200um and 400um from each surface, respectively. This asymmetric

trend was noted within the x-ray diffraction surface measurement results, however in terms of near surface compressive stress magnitude, rather than depth of compressive residual stress penetration. This again may be attributable to surface roughness differential prior to the peening process, or cold through thickness wave propagation working during the staged peening process (peen flip peen).

CHAPTER 6.

6.1 SEM Imaging

6.1.1 Hypothesis

Through this experimentation, this thesis endeavors to answer the question of what is the mechanism for shot peening enhancement for fatigue performance. An objective of this work is to understand how a cracked particle starts to incubate the short crack into the matrix within a residual stress field, and at what stage of the fatigue life this occurs, and if shot peening has an effect upon the phenomenon.

6.1.2 Effect of Shot Peening Process on Secondary Phase

A key element of this research is to understand how a cracked particle starts to incubate the short crack into the matrix within a residual stress field. The critical difference in this research hypothesis, is the existence of shot peened cracked precipitates, prior to any fatigue cycling. The shot peening of the substrate causes plastic-elastic deformation and induces a compressive residual stress field, however, detrimentally cracks hard constituent precipitate particles, as well as inducing surface damage. Limited literature exists to quantify the extent of this cracking, however, Hochhalter, *et al*,[56] have conducted statistical analysis upon the cracking state of cracking of constituent particles (precipitates) of baseline AA7075-T651 following fatigue. To the knowledge of the author, no precipitate cracking assessment of shot peened constituent particles has been carried out.

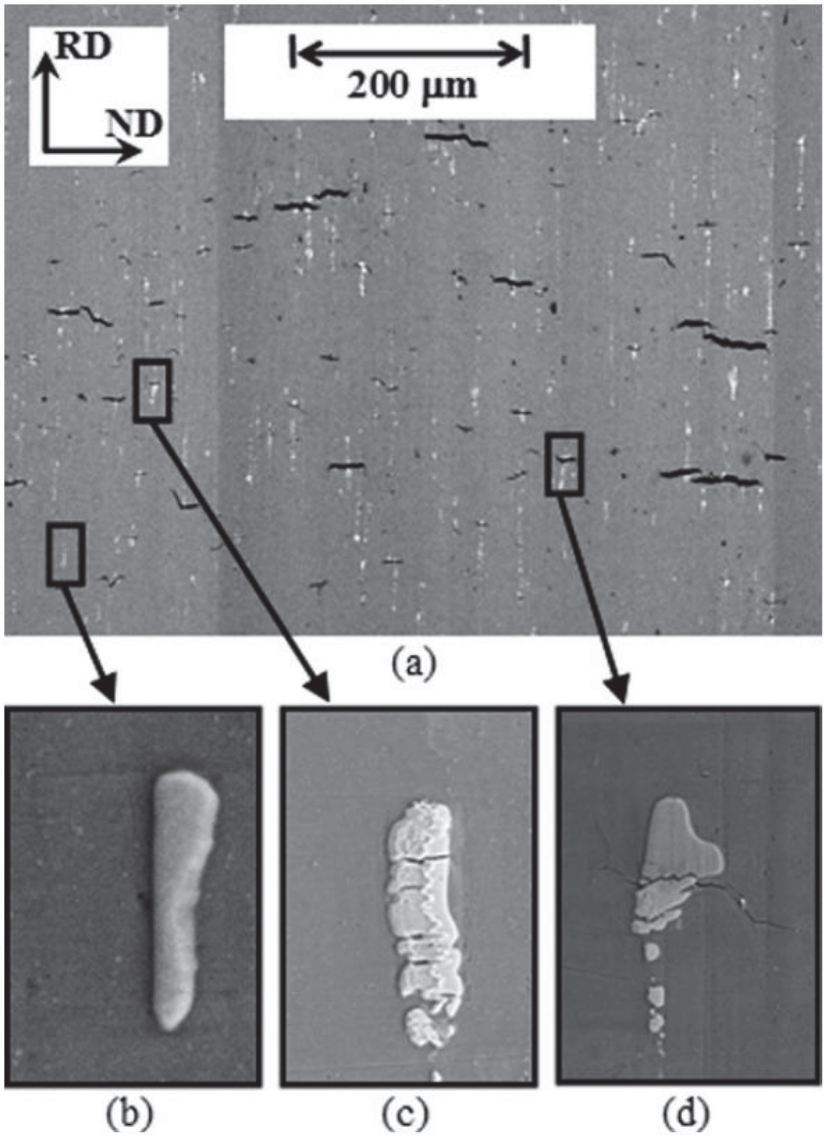

Figure 45 By Hochhalter, et al;[57] (a) SEM image of AA7075-T651 under load, showing cracking. Images show (b) an uncracked precipitate, (c) a cracked precipitate where the crack did not extend into the matrix, and (d) a cracked precipitate with the crack extending into the matrix.

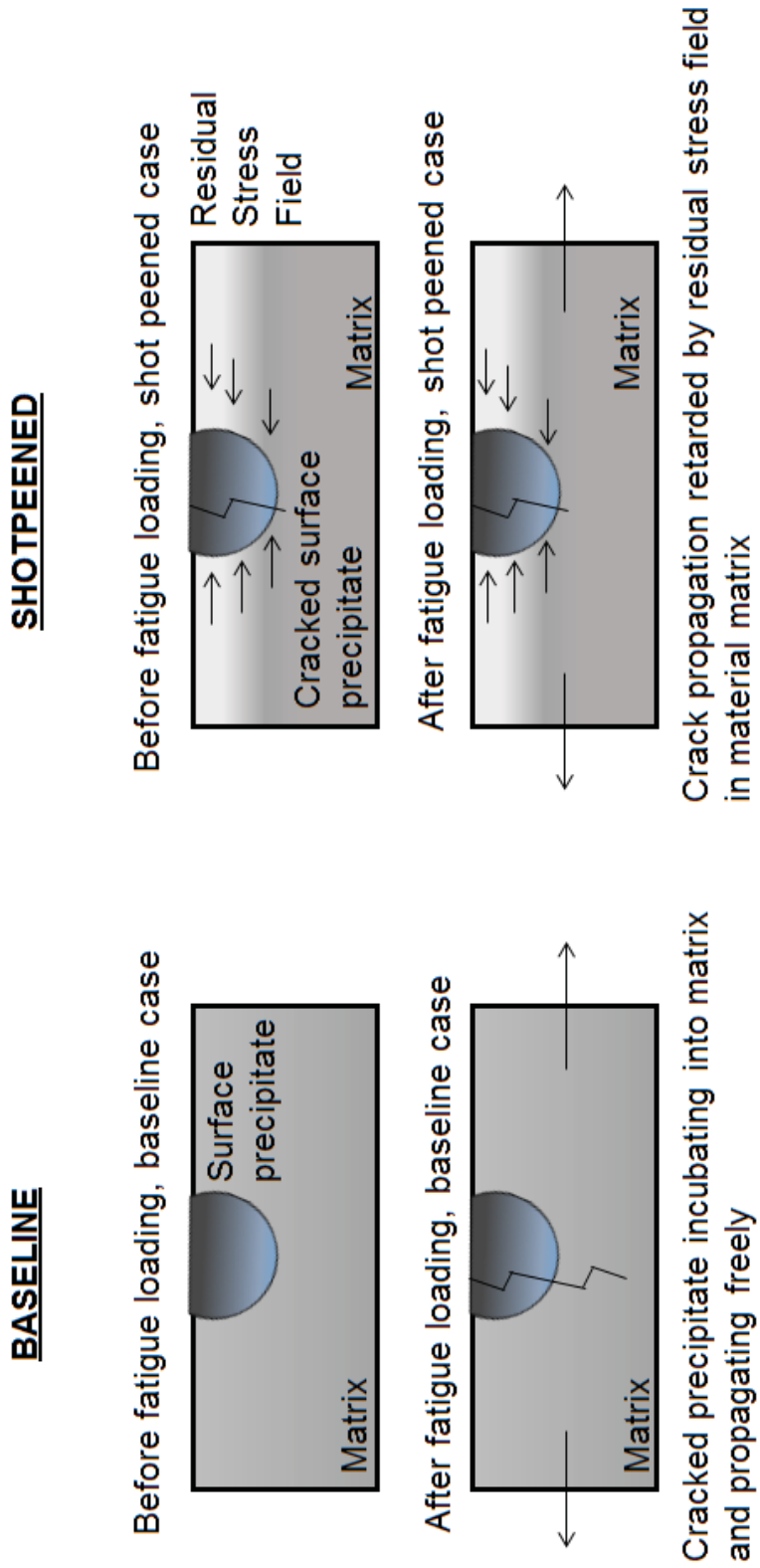

Figure 46 Comparison of theorized precipitate cracking state, baseline and shot peened samples, before and after fatigue loading.

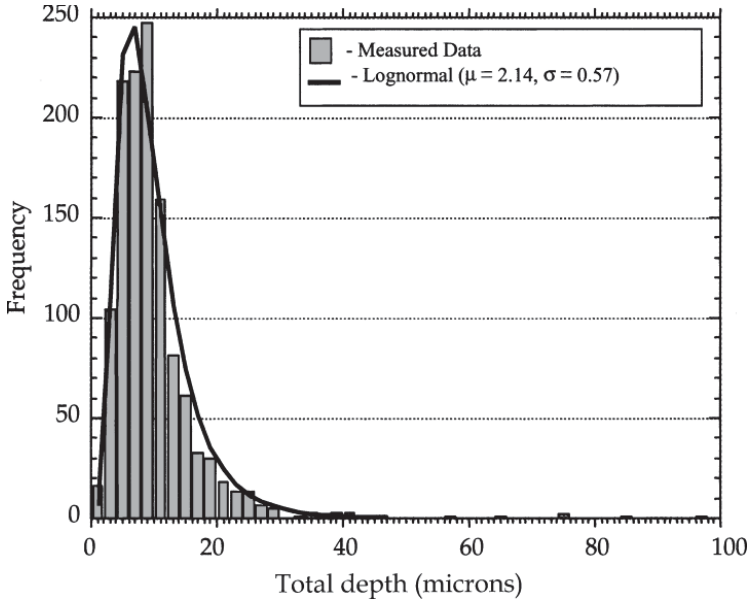

Figure 47 Sharp *et al*[58], demonstrate the subsurface distribution of precipitates that initiated fatigue cracking in baseline AA7050-T7451.

Sharpe *et al*, suggest that material imperfections play a significant role in the early stages of fatigue cracking (incubation, nucleation), with precipitates being a common site for fatigue crack initiation. A survey conducted upon approximately a thousand fatigue cracks within baseline AA7050-T7451, noted the depth of the inclusion from which a crack initiated. The survey suggests that for a fatigue regime, that a majority of fatigue cracking initiating from precipitates, is concentrated at the 10um sub surface (when the fatigue is conducted).

With this in mind, therein lies the potential to qualitatively analyze the competing effects of shot peening, inducing a compressive residual stress, and cracking particles, through the fatigue life.

6.1.3 SEM Evaluation: Before and After Fatigue Precipitate State

The following images were obtained using a FEI Philips XL-40 SEM. Considerations when surveying and analyzing the precipitate states, include the extent of the cracking, voids in the vicinity of the precipitate, the proximity of the precipitate to the machining surface (and in the peened case, the peening surface). Surveys of precipitates were carried out in the following four states:

1. Shot peened sample before fatigue;
    - Polished to a uniform depth of approximately 90um beneath shot peening surface (important relevant to subsurface precipitate cracking).
2. Shot peened sample after fatigue (4.5k cycles);
    - Polished to a uniform depth of approximately 100um beneath shot peening surface.
    - Fatigued to n=4,500 cycles, under parameters detailed at Chapter 5.
3. Basline sample before fatigue;
    - Polished to a uniform depth of 400um below machining surface.
4. Baseline sample after fatigue (5.5k cycles);
    - Polished to a uniform depth of 400um below machining surface.
    - Fatigued to n=5,500 cycles, under parameters detailed at Chapter 5.

6.1.4 Shot Peened Survey

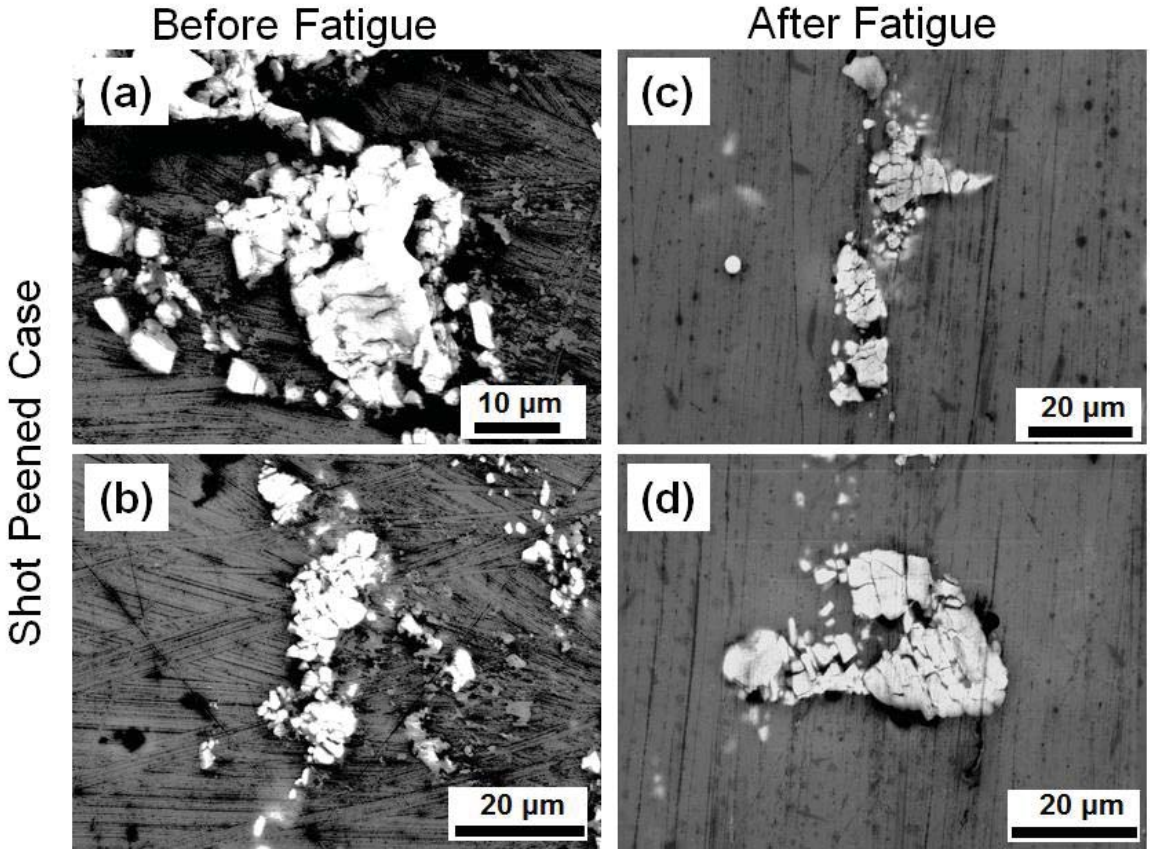

Figure 48 SEM image of AA7050-T7451 following the shot peening process. Images show (a) an cracked precipitate (90um subsurface) before fatigue, (b) a cracked precipitate (90um subsurface) before fatigue, (c) a cracked precipitate (100um subsurface) following fatigue, and (d) a cracked precipitate (100um subsurface) following fatigue with evidence of de-banding.

It should be qualitatively noted that during SEM image surveying, that in both shot peened state 1 and 2 (shot peened before and after fatigue), that all precipitates showed evidence of cracking within the precipitate itself. Following fatigue, the cracked precipitates are observed to be obliterated, with significant cracking throughout. It is interesting to note that only minor de-bonding occurred with reference to the precipitate interaction with the matrix, without evidence of cracking extending into the material matrix itself. It is theorized, that the absence of this cracking extending into the matrix is due to the

compressive residual stress field induced by shot peening, retarding the crack propagation into the material matrix; combined with the effect of cracked precipitates having a higher compliance due to the initially cracked state of all the shot peened sample precipitates.

6.1.5 Baseline Survey

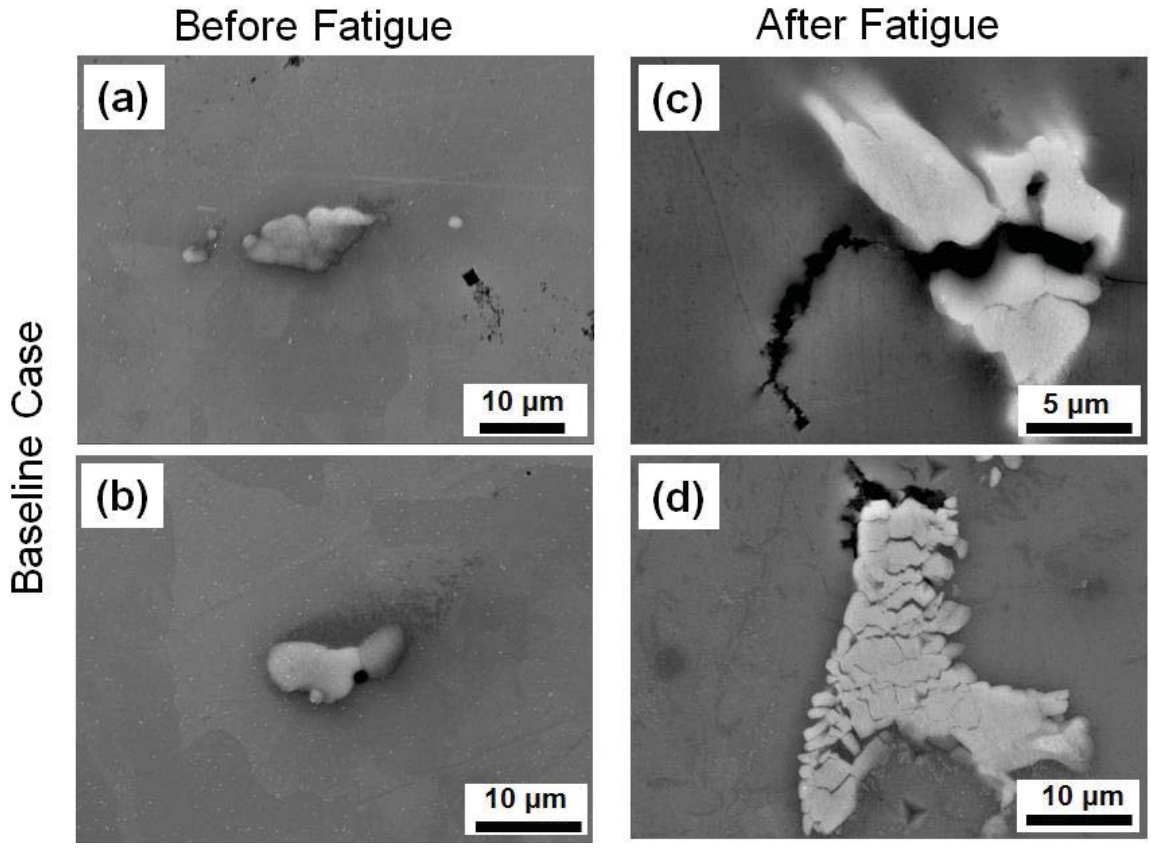

Figure 49 SEM image of AA7050-T7451 in the baseline condition. Images show (a) an intact precipitate (400um subsurface) before fatigue, (b) an intact precipitate (400um subsurface) before fatigue, (c) a cracked precipitate demonstrating incubation and propagation into the material matrix following fatigue, (d) an obliterated precipitate demonstrating de-banding and crack propagation into the material matrix.

It should be qualitatively noted that some cracking was evident during the surveying of baseline state 3 (before fatigue), that some precipitates were cracked and uncracked. Following the fatigue regime, the precipitates are observed to exhibit significant cracking, and incubation of said cracks into the material matrix, including propagation. The absence of any compressive residual stress field within the matrix, unlike the shot peened case, results in propagation of the cracking extending into and throughout the substrate.

6.1.6 Discussion

This survey has provided qualitative evidence to suggest that despite the fact shot peening may initially crack precipitate particles, this detrimental effect is somewhat offset by the induced compressive residual stress induced by the process. Further in situ observation of crack initiation and propagation in the two cases could be carried out to improve the understanding of the precipitate to matrix interaction, with regard to fatigue crack initiation within the material matrix, comparing the baseline and shot peened state.

6.2 Nano-Indentation

The following element of this research was carried out in co-operation with Siavash Ghanbari under the supervision of Prof. Bahr, and the Materials Engineering Department's Center for Surface Engineering and Enhancement.

6.2.1 Precipitate Mapping

In order to evaluate the precipitate state and surrounding material matrix, as per the hypothesized cracking effect during shot peening and fatigue, a line nano-indentation regime was developed. The regime involved the identification of target precipitates within a known area of interest via optical imaging, following surface preparation carried out as detailed in Chapter 3. Optical imaging maps of each area were taken using an Olympus BX51M optical microscope, showing location of precipitates, on a shot peened and baseline sample, prior to fatigue at 10x magnification.

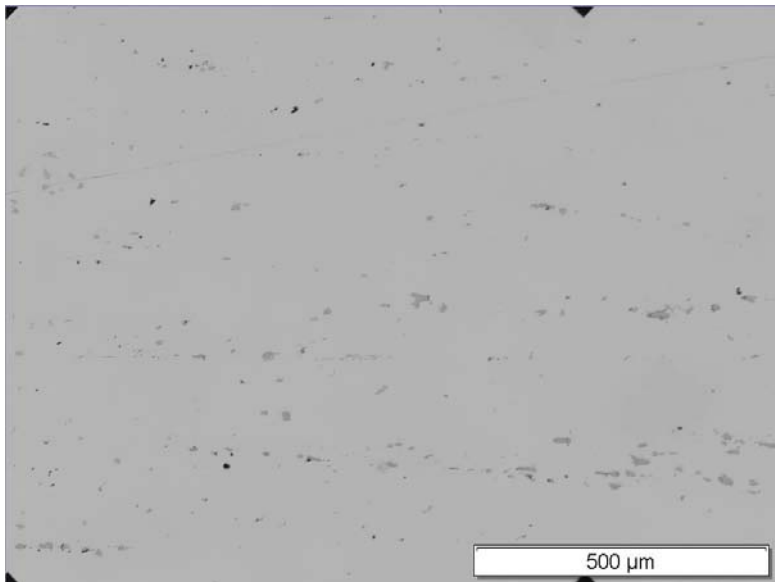

Figure 50 Optical microscope precipitate map of a baseline sample at 10x magnification, illustrating precipitates readily identifiable within the material matrix.

6.2.2 Nano-indentation Experimentation

The intention of the nano-indentation was to evaluate the precipitate compliance, in addition to the relative residual stress of the material matrix surrounding the precipitate.

Once precipitate locations were identified, samples were then mounted for nano-indentation, again utilizing a Hysitron TI950 TribIndenter, in conjunction with a Berkovich pyramid indentation tip. The indentation procedure involves the penetration of a flat, uniform surface of the analyzed substrate with the indentation tip.

Nano-indentation was carried out on precipitates before and after, fatigue, on a shot peened sample, and baseline sample, in the following states, identical to the SEM survey:

1. Shot peened sample before fatigue;
    - Polished to a uniform depth of approximately 90um beneath shot peening surface (important relevant to subsurface precipitate cracking).
2. Shot peened sample after fatigue (4.5k cycles);
    - Polished to a uniform depth of approximately 100um beneath shot peening surface.
    - Fatigued to n=4,500 cycles, under parameters detailed at Chapter 5.
3. Basline sample before fatigue;
    - Polished to a unifrom depth of 400um below maching surface.
4. Basline sample after fatigue (5.5k cycles);
    - Polished to a unform depth of 400um below maching surface.
    - Fatigued to n=5,500 cycles, under parameters detailed at Chapter 5.

In each state, nano-indentation was conducted within single area of interest upon precipitates within the area of interest. Indentation pattern was in a straight line and each

with a spacing of 10um, spanning enough interrogation points to traverse from one side of the precipitate within the material matrix, to the opposite side (usually involving 7-10 indents). It was attempted to place the central indents of the line, directly upon the precipitate center.

Figure 51 illustrates the line indentation pattern, of which was utilized to interrogate both the precipitate, and surrounding material matrix.

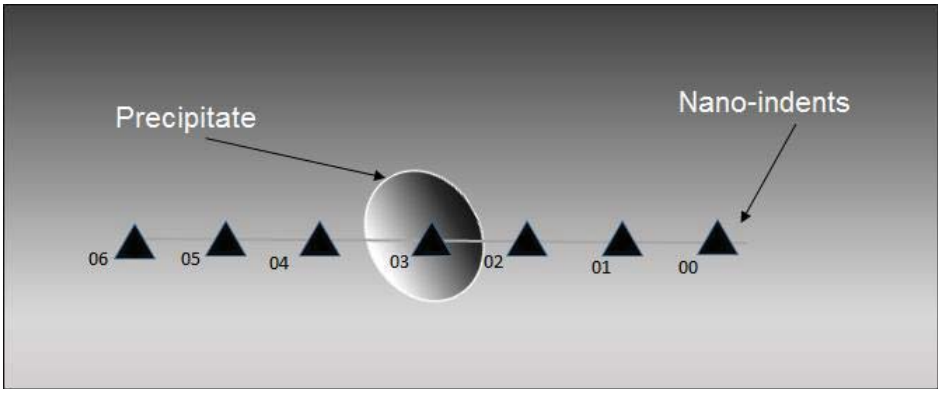

Figure 51 Line pattern of indentation utilized to interrogate precipitate particles, including 7 indents at 10um spacing.

6.2.3 Anticipated Results

Based upon the hypothesis cracking state, and the SEM imaging survey, it was anticipated that the precipitate hardness magnitude would following the order, in decreasing hardness: baseline before fatigue, shot peened before fatigue, baseline after fatigue, and shot peened after fatigue. This was presumed based upon the anticipated response to the precipitate cracking state illustrated within Figure 46, and the expected compliance of the respective precipitate areas whilst undergoing nano-indentation, due to precipitate cracking.

6.2.4 Results – Matrix Residual Stress

In order to appropriately present results, the Suresh and Giannakopoulos model should understood. In representing the qualitative residual stress of the material matrix for the states of the samples, the indentation load versus indent penetration depth must be graphically explained.

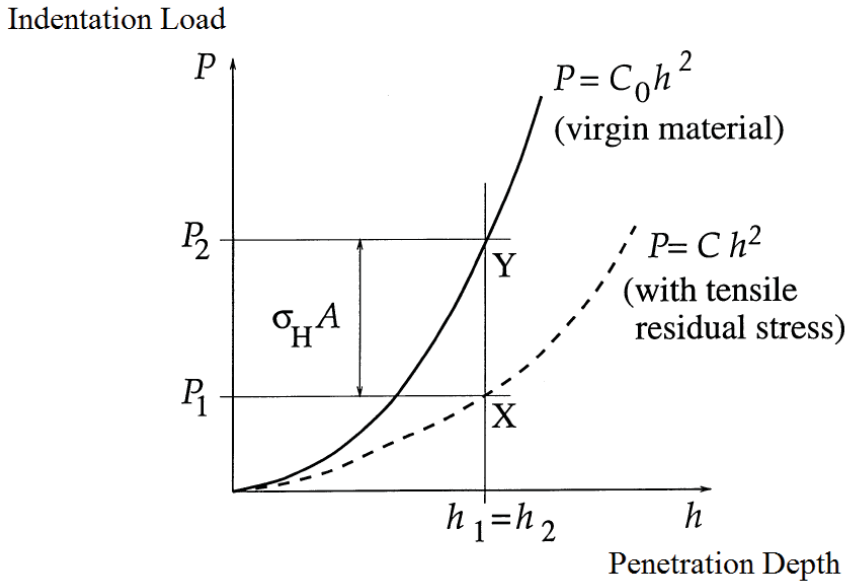

Figure 52 Suresh and Giannakopoulos indentation load versus penetration depth curve for the qualitative estimation of residual stress by nano-indentation.[59]

Figure 52 illustrates the translation in the indentation load versus penetration depth curve for a tensile residual stress, in comparison to a stress free virgin material. We note that for a tensile residual stress, a shift downward and to the right on the plot. For a compressive residual stress, a similar translation occurs, however upwards and to the left of the stress free (virgin material) curve. These shifts are further detailed by Suresh and Giannakopoulos, however for the intention of displaying qualitative changes in residual stress for the material matrix, this level of understanding is suffice.

In the representation of residual stress for the material matrix, only indents clearly within the matrix were utilized as data points. Figure 53 illustrates the material matrix qualitative residual stress measurement resulting from nano-indentation.

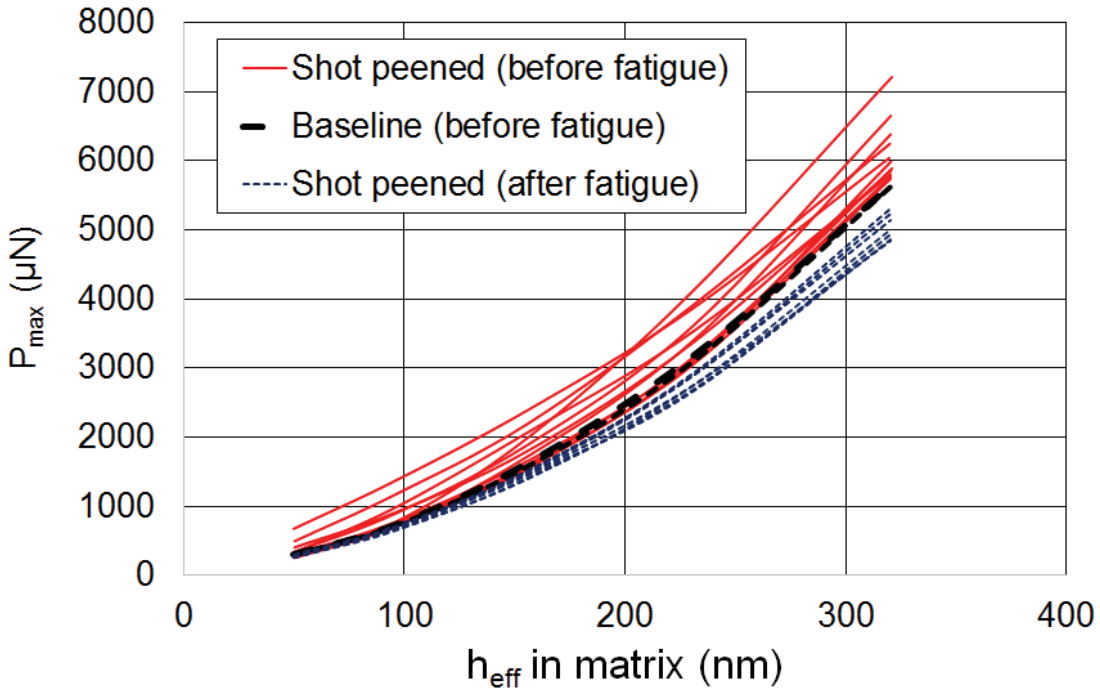

Figure 53 The indentation load versus penetration depth curve for shot peened samples, compared with a presumed stress free baseline material, illustrating the compressive residual stress before fatigue.

Figure 53 illustrates a compressive residual stress bias for the shot peened sample, prior to fatigue. This is expected, and correlates with theory and x-ray diffraction results. Additionally, we see a relaxation through fatigue, with the shot peened sample curves in an orientation closer to the stress free state than the compressive residual stress observed in the pre-fatigue case.

6.2.5 Precipitate Particles – Nano-indentation Modulus Evaluation

In addition to deriving the residual stress of the material matrix, the precipitates were evaluated as per the hypothesized cracking state via quantification of modulus from the indentation loading and unloading data. This practice was carried out utilizing the theoretical methodology described by Oliver and Pharr.[60] The nature of nano-indentation allows for the measurement of modulus at a very precise location, ideal for interrogating individual precipitates on the micrometer scale. From imaging obtained during the indentation process, indentation data points were selected based on location relative to the precipitates. For evaluation of modulus, only data points clearly within the boundary of the precipitate were selected as representative.

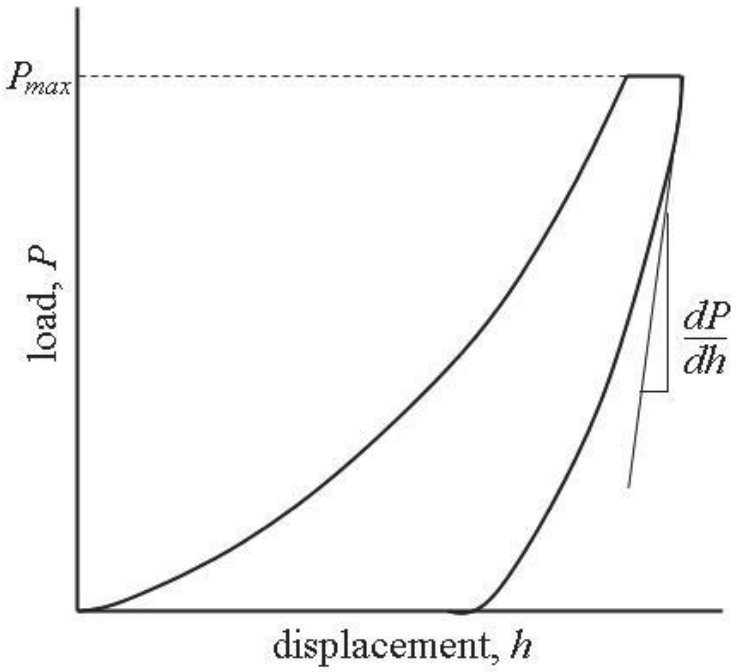

Figure 54 The indent load versus depth curve, illustrating the gradient of the unload section of the curve, utilized in deriving the indented material modulus.[61]

Oliver and Pharr describe the theoretical methodology for which the reduced modulus is derived from nano-indentation testing data. The gradient of the unloading during the indentation test is indicative of the reduced modulus, which, with the resultant test information, combined with material/indenter geometric contact information, gives the material reduced modulus. Figure 55 illustrates the resultant reduced modulus distribution for the tested precipitate states.

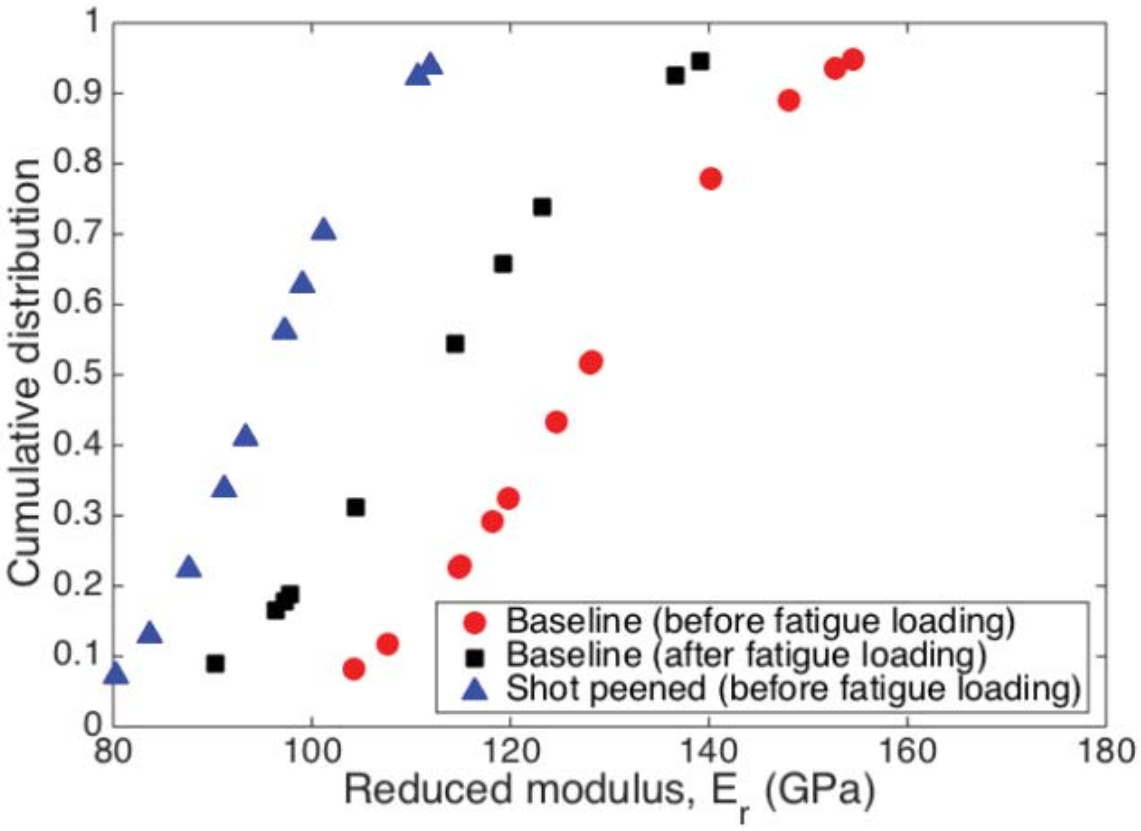

Figure 55 Cumulative distribution of the reduced modulus of sample states, illustrating a higher modulus prior to fatigue

6.2.6 Discussion

It can be seen from Figure 55, that there is a distinct qualitative trend, in terms of the resulting reduced modulus for each precipitate state. The shot peened reduced modulus is at the lower end of the spectrum, then followed by the baseline post fatigue state, and finally the baseline pre fatigue state. This order of modulus is qualitatively in agreement with the hypothesized cracking state, whereby, it is assumed that a higher extent of cracking within the precipitate particle, will result in a lower compliance (low elastic modulus).

CHAPTER 7.

7.1 Summary

This work has provided the foundation for future continued investigative research into crack initiation and crack incubation by precipitates within shot peened aluminum alloys, specifically AA7050-T7451. Surface topography following shot peening has been measured. Grain characterization has been carried out, noting no discernable difference in microstructure between shot peened and baseline samples in terms of grain size at a sub-peening depth of approximately 90um. Elemental analysis has been carried out, demonstrating the chemical constituents of precipitate particles within AA7050-T7451 are predominantly comprised of Al_7Cu_2Fe. A fatigue performance comparison has been conducted, with the small batch of shot peened samples, with no discernable difference in fatigue performance concluded when compared to baseline samples.

A significant outcome of this thesis, is the hypothesized cracked versus uncracked state of precipitate particles with AA7050-T7451. The effect of shot peening upon the state of precipitates has been considered, demonstrating that subsurface particle cracking is evident via surface preparation and SEM imaging of precipitates in shot peened samples. Near surface residual stresses have been evaluated through x-ray diffraction measurement in shot peened samples, as a function of fatigue, demonstrating rapid relaxation of near surface residual stresses leading to the reduction in beneficial (crack retardation) residual

compressive stress, and subsequently failure at a similar fatigue performance (number of cycles) under identical stress controlled loading parameters to that of baseline samples.

The scanning electron microscope survey of precipitates confirmed the cracked state of precipitates in the shot peened samples, prior to fatigue loading, demonstrating the adverse effect of shot peening damage. This cracked state has been quantified utilizing experimental nano-indentation techniques in cooperation with the Center for Surface Engineering and Enhancement. Additionally, the qualitative through thickness residual stress profile of shot peened samples have been generated utilizing a nano-indentation technique in combination with the Suresh Giannakopoulos model.

7.2 Recommendations and Future Work

Further work should be concentrated on the little understood area of the effect of shot peening on hard precipitates within the material matrix. Some fundamental qualitative results have shown there is potential for further work, and possibly an optimization study, into the trade-off in fatigue performance between surface enhancement via compressive residual stressing, and cracking of precipitate particles through shot peening.

A larger sample batch size for AA7050-T7451 fatigue analysis could be evaluated for baseline versus shot peened fatigue performance comparison, to either evaluate the fatigue performance under the fatigue parameters used in this study, or, alternatively, in a high cycle fatigue regime, in order for the crack propagation retardation effect of the shot peened residual stress profile to have a more profound effect upon fatigue performance.

Another interesting future endeavor could involve the comparative in situ analysis of precipitate cracking, incubation, and propagation of shot peened and baseline samples from the constituent precipitate particles.

This nature of work would benefit from larger specimens, on which a higher cycle fatigue regime could be conducted.

Another variation which has potential to improve the understanding of the effect of shot peening on the cracking of precipitates is to incorporate FIB (Fine Ion Beam) polishing techniques into the surface preparation regime. This process would allow for more precise surface preparation, and analysis in closer proximity to the shot peened surface.

Finally, there exists the potential of the variation in Almen intensity, and the subsequent effect upon the cracking of precipitates, and resultant material performance, to be evaluated.

REFERENCES

REFERENCES

[1] P.K. Sharp and G. Clark, "The Effect of Peening on the Fatigue Life of 7050 Aluminum Alloy", *DSTO Aeronautical and Maritime Research Laboratory*, 2001, p. 01.

[2] G.F. Bush, J.O. Almen, L.A. Danse, J.P. Heise, "How, When and By Whom was Mechanical Prestressing Discovered?", *Society of Automotive Engineers, ISTC Div. 20*, 1962.

[3] Sumerian Shakespear, [Online], "Weapons Found in the Royal Tombs of Ur", http://sumerianshakespeare.com/117701/118301.html, accessed 05 Oct 2016.

[4] J. Johnson, J. Johnson, A. Whetstone, [Online] "Peening Poster", http://www.webpages.uidaho.edu/mindworks/machine_design/posters/pdf/peening_poster.pdf, accessed 05 Oct 2016.

[5] P.E. Cary, "History of Shot Peening", *The Shotpeener Library*, Article 1981028, 1981, pp. 23-26.

[6] D. Kirk, "Shot Peening", *Aircraft Engineering and Aerospace Technology; An International Journal,* Vol. 71 No4, 1991, pp. 349-362.

[7] D. Kirk, "Shot Peening", 1991, p. 349.

[8] D. Kirk, "Shot Peening", 1991, p. 350.

[9] D. Kirk, "Residual Stresses in Shot Peened Components", *The Shot Peener Library*, Article 2004003, 2004, p. 01.

[10] W. Elber, "The Effects of Shot Peening Residual Stresses on the Fracture and Crack Growth Properties of D6AC Steel", *National Aeronautics and Space Administration Langley Research Centre*, Report No. TM X-71943.

[11] D. Kirk, "Residual Stresses in Shot Peened Components", 2004, p. 07.

[12] Progressive Surface, [Online] "Shot Peening: What is Shot Peening?", http://www.progressivesurface.com/shotpeening_process.php, accessed 15 Oct 16.

[13] Curtis-Wright, [Online] "Controlled Shot Peening", http://www.cwst.co.uk/services/controlled-shot-peening/, accessed 12 Sep 16.

[14] D. Kirk, “Estimate Compressed Layer Depth by Using Almen Peening Intensity”, *The Shot Peener,* 2014, pp. 30-38.

[15] D. Kirk, “Shot Peening”, 1991, p. 351.

[16] D. Kirk, “Shot Peening”, 1991, p. 350.

[17] P.K. Sharp and G. Clark, “The Effect of Peening on the Fatigue Life of 7050 Aluminum Alloy”, p. 02.

[18] P.K. Sharp and G. Clark, “The Effect of Peening on the Fatigue Life of 7050 Aluminum Alloy”, p. 01.

[19] P.K. Sharp and G. Clark, “The Effect of Peening on the Fatigue Life of 7050 Aluminum Alloy”, p. 01.

[20] J.Q. Clayton, G. Clark, “The Effect of Steel Shot and Glass Bead Peening Treatments on the Fatigue Resistance of 7050-T76351 Aluminum Alloy”, *Fracture Mechanics in Engineering Practice, Melbourne,* 1988, pp44-51.

[21] P.K. Sharp and G. Clark, “The Effect of Peening on the Fatigue Life of 7050 Aluminum Alloy”, p. 53.

[22] A.G. Broulidakis, “A Model for the Prediction of Residual Stresses Resulting from Shot Peening and its Incorporation into the ANSYS Finite Element Solver”, *Rensselaer Polytechnic Institute,* 2013, p. 07.

[23] Surfex – Surface Finishing Equipment Company, [Online] “Other Products and Accessories”, http://surfex.in/other-products-accessories-of-shot-peening/, accessed 19 Nov 16.

[24] P.K. Sharp and G. Clark, “The Effect of Peening on the Fatigue Life of 7050 Aluminum Alloy”, p. 03.

[25] P.K. Sharp and G. Clark, “The Effect of Peening on the Fatigue Life of 7050 Aluminum Alloy”, p. 03.

[26] Society of Automotive Engineers, “Aerospace Material Specification – AMS 4050 Aluminum Alloy Plate (7050-T7451)”, *Society of Automotive Engineers,* 1974.

[27] Department of Defense Handbook MIL-HBBK-5J, “Metallic Materials and Elements for Aerospace Vehicle Structures”, *Department of Defense United States of America,* 2003.

[28] Aloca Mill Products, “Alloy 7050 Plate and Sheet: Best Combination of Properties”, *Catalog Number E22-14752.*

[29] ASM Aerospace Specification Metals Inc, [Online] “Aluminum 7050-T7541 (7050-T73651)”, http://asm.matweb.com/search/SpecificMaterial.asp?bassnum=MA7050T745, accessed 15 Oct 2016.

[30] ASM Aerospace Specification Metals Inc, [Online] "Aluminum 7050-T7541 (7050-T73651)", accessed 15 Oct 16.

[31] D.J. Chadwick, "2D Axisymmetric Model for Prediction of Residual Stress Profile from Shot Peening", *Purdue University AAE558*, Fall Semester 2015.

[32] R. Howard, "A Study in the Prediction of Residual Stresses in Shot Peening", *Rensselaer Polytechnic Institute Hartford*, 2008.

[33] X.L. Fu, "Constitutive Equation for 7050 Aluminum Alloy - Johnson-Cook Constitutive Model", *School of Mechanical Engineering Shandong University*, 2006.

[34] Howard, "A Study in the Prediction of Residual Stresses in Shot Peening*"*, 2008.

[35] A.W. Mello, A. Nicolas, M.D. Sangid, et al, "Effect of Microstructure on Strain Localization in a 7050 Aluminum Alloy: Comparison of Experiments and Modeling for Various Textures", *Materials Science and Engineering*, Vol. 661, 2016, pp 187-197.

[36] ASTM E8/E8M-13a, "Standard Test Methods for Tension Testing of Metallic Materials", *ASTM International*, 2013, pp. 01-28.

[37] A.W. Mello, A. Nicolas, M.D. Sangid, et al, "Effect of Microstructure on Strain Localization in a 7050 Aluminum Alloy: Comparison of Experiments and Modeling for Various Textures", 2016.

[38] S. Nasseri, "The Nature of Materials: Manufacturing Processes", *Southern Polytechnic State University Press*, 2014.

[39] A. Winkelmann, C. Trager-Cowan, F. Sweeny et al, "Many-beam Dynamical Simulation of Electron Back Scatter Diffraction Patterns", *Science Direct - Ultramicroscopy 107*, 2006, pp. 414-421.

[40] A. Winkelmann, C. Trager-Cowan, F. Sweeny et al, "Many-beam Dynamical Simulation of Electron Back Scatter Diffraction Patterns", 2007, p.415.

[41] EDAX Inc, "Technical Note – EBSD: Confidence Index", Ameteck Materials Analysis Division, 2013.

[42] Y. Harada, K. Fukaura, N. Tsuchida, "Grain Refinement of Metal Surface Using Hot Shot Peening", *Materials Science Forum ISSN: 1622-9752 Vols. 539-543, Trans Tech Publications,* 2007, pp. 1080-1085.

[43] J. Root, "Elemental Analysis (EDS) on the XL-40", *Purdue University Instructional and Research Support Engineer Guide Notes*, Purdue University, 2016.

[44] A.W. Mello, A. Nicolas, M.D. Sangid, et al, "Effect of Microstructure on Strain Localization in a 7050 Aluminum Alloy: Comparison of Experiments and Modeling for Various Textures", Materials Science and Engineering A, Vol. 661, 2016, pp 187-197.

[45] International Organization for Standardization, "ISO 1099 Metallic Materials – Fatigue Testing – Axial Force Controlled Method", *ISO Switzerland,* 2006.

[46] H.P Lieurade, A. Bigninnet, "Fundamental Aspects of the Effect of Shot Peening on the Fatigue Strength of Metallic Parts and Structures", *IRSID 78105 St-Germain-en-Laye France,* 1987

[47] M.E. Fitzpatrick, A.T. Fry, P. Holdway et al, "Determination of Residual Stresses by X-ray Diffraction – Issue 2", *Measurement Good Practice Guide,* No. 52, 2005, p. 01.

[48] P.S. Prevey, "X-Ray Diffraction Residual Stress Techniques", *Lambda Technologies, Metals Handbook 10 Metals Park: American Society for Metals,* 1986, p.382.

[49] P.S. Prevey, "X-Ray Diffraction Residual Stress Techniques", 1986, p.382.

[50] P.S. Prevey, "X-Ray Diffraction Residual Stress Techniques", 1986, p.382.

[51] P.S. Prevey, "X-Ray Diffraction Residual Stress Techniques", 1986, p.382.

[52] P.S. Prevey, "X-Ray Diffraction Residual Stress Techniques", 1986, p.382.

[53] P.K. Sharp and G. Clark, "The Effect of Peening on the Fatigue Life of 7050 Aluminum Alloy", 2001.

[54] S. Suresh, A.E. Giannakopoulos, "A New Method for Estimating Residual Stress by Instrumented Sharp Indentation", *Acta Mater, Vol 46, No. 16,* 1998, pp. 5755-5767.

[55] S. Suresh, A.E. Giannakopoulos, "A New Method for Estimating Residual Stress by Instrumented Sharp Indentation", *Acta Mater, Vol 46, No. 16,* 1998, p. 5756-5757.

[56] J.D. Hochhalter, et al, "A Geometrical Approach to Modeling Microstructually Small Fatigue Crack Formation: I. Probabilistic Simulation of Constituent Particle Cracking in AA7075-T651", *Modelling and Simulation in Materials Science and Engineering, IOP Publishing,* 2008, p. 04.

[57] J.D. Hochhalter, et al, "A Geometrical Approach to Modeling Microstructually Small Fatigue Crack Formation: I. Probabilistic Simulation of Constituent Particle Cracking in AA7075-T651", 2008, p. 04.

[58] S.A Barter, P.K. Sharp, G. Holden, G. Clark, "Initiation and Early Growth of Fatigue Cracks in an Aerospace Aluminum Alloy", *Fatigue and Fracture of Engineering Materials and Structures* 2002; 25: pp. 111-25.

[59] S. Suresh, A.E. Giannakopoulos, "A New Method for Estimating Residual Stress by Instrumented Sharp Indentation", *Acta Mater, Vol 46, No. 16,* 1998, p5759.

[60] W.C. Oliver, G.M. Pharr, “Measurement of Hardness and Elastic Modulus by Instrumented Indentation: Advances in Understanding”, *Journal of Materials Research, Vol. 19, No. 1,* 2004.

[61] Wikipedia, [Online], “Nanoindentation”, https://en.wikipedia.org/wiki/Nanoindentation, accessed 27 Nov 16.